



CHAPTER IV

RESULTS AND DISCUSSION

From the previous work (Khaikham, 2007), the deactivation of the adsorbents was investigated in low degrees of less than 20% deactivation, particularly the 1/8" and 1/16" 4A molecular sieve. Therefore, to study the changes of both adsorption isotherm and breakthrough time at high percentages, i.e. more than 20%, of deactivation, both adsorbents were acceleratingly aged under hydrothermal conditions. The characterizations of the adsorbents were conducted to understand the changes in the physical properties of the adsorbents caused by their deactivation. Moreover, the parameters in the mass balance equation and the water adsorption isotherms of adsorbents changing with the percentage of deactivation were determined to be used in the mass balance equation for the estimation of breakthrough time.

4.1 Static Adsorption Capacity of Adsorbents

The adsorption capacity of the 1/8" and 1/16" 4A molecular sieve was investigated by using TG/DTA. The total weight loss of water-saturated adsorbents is the static adsorption capacity.

During the service of the adsorbents, they gradually lose their capacity, thus the static adsorption capacity of deactivated adsorbents needs to be studied. Normally, in the system which has an absence of water, the zeolites are stable at high temperature, but in this work the water is an impurity, which is adsorbed on the adsorbent and in the regeneration step hot gas is used to remove that water from the adsorbent. Thus, this system has both heat and water, which is known as a hydrothermal system with the result that deactivation can occur easily. So, to study this effect, the adsorbent aging was accelerated under hydrothermal conditions by boiling the adsorbent at 600°C and the number of batches was varied to increase the aging of adsorbent. The capacity of both adsorbents varied with the number of batches is shown in Tables 4.1 and 4.2 below.

Table 4.1 Static adsorption capacities of the fresh and deactivated 1/8" 4A molecular sieve at 100% RH and 25°C

Number of batches	Adsorption capacity (g water/100g adsorbent)	%deactivation
fresh	26.75	0
5	23.71	11.36
15	14.38	46.24
25	12.31	53.98
35	9.25	65.42
45	7.02	73.75

Table 4.2 Static adsorption capacities of the fresh and deactivated 1/16" 4A molecular sieve at 100% RH and 25°C

Number of batches	Adsorption capacity (g water/100g adsorbent)	%deactivation
fresh	26.75	0
5	24.62	7.96
15	10.06	62.39
25	9.64	63.96
35	9.08	66.06
45	4.56	82.95

From the above tables, the adsorption capacity decreasing with the number of batches was obtained from the changes of the total weight loss of both adsorbents saturated with water, as shown in Figures 4.1 and 4.2.

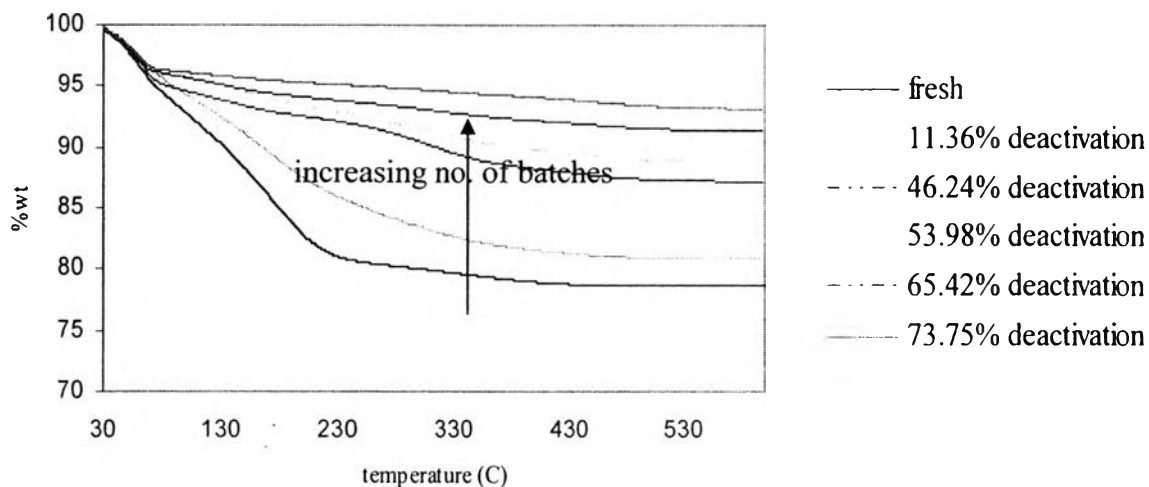


Figure 4.1 Weight loss of fresh and deactivated 1/8" 4A molecular sieve saturated with water obtained from TG/DTA experiments.

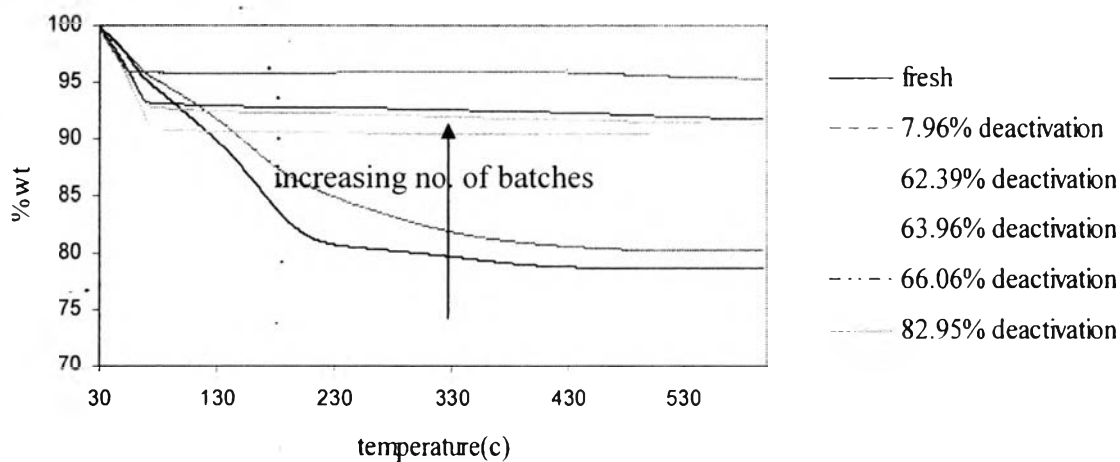


Figure 4.2 Weight loss of fresh and deactivated 1/16" 4A molecular sieve saturated with water obtained from TG/DTA experiments.

From Figures 4.1 and 4.2, even though the weight of the adsorbents continually decreases until to 550°C, most of the weight loss occurs below 350°C, which is about 97% of all weight loss of the adsorbents. Even though 550°C is the temperature at which nearly all of the water can be removed, it is not the proper temperature for the regeneration step because deactivation can occur quickly. So,

175-300°C was recommended in order to save the life of the adsorbent (Campbell, 1984).

If the percentage of deactivation between the small size and big size 4A molecular sieve under the same condition is compared, it is found that the small one is easier to deactivate than the big one. Because the small size 4A molecular sieve exposes higher surface area to the system under hydrothermal conditions and heat can transfer into the pellet better than the big size 4A molecular sieve, so it was easily destroyed.

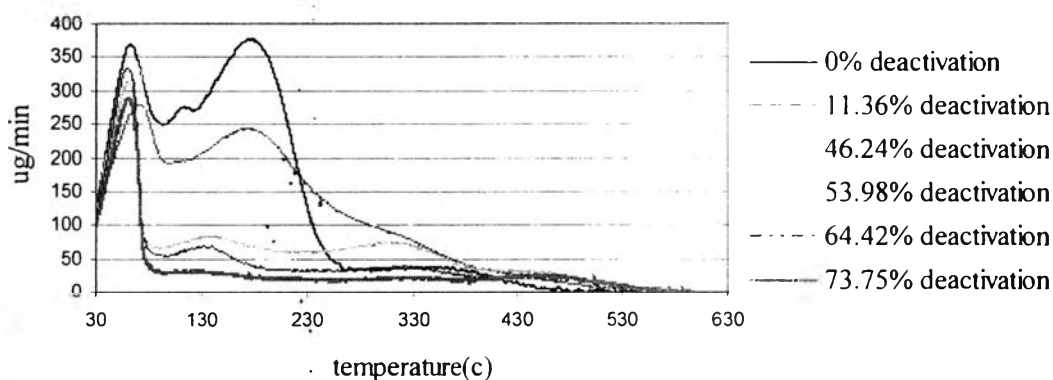


Figure 4.3 Weight loss derivative of fresh and deactivated 1/8" 4A molecular sieve obtained from TG/DTA.

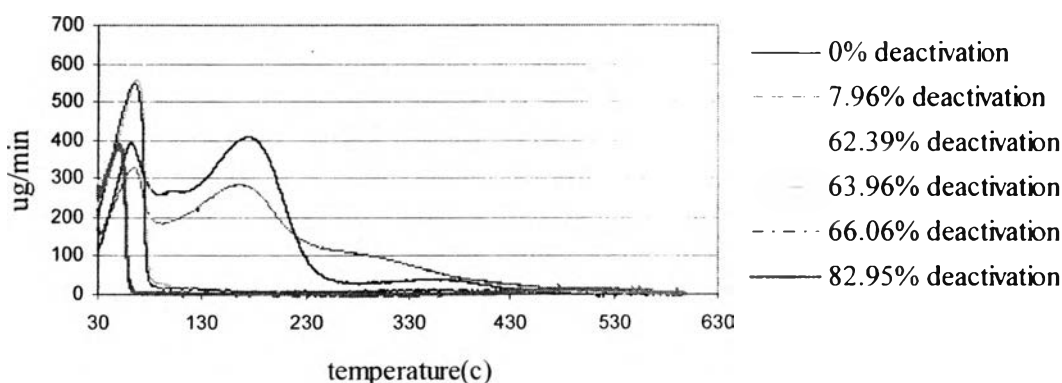


Figure 4.4 Weight loss derivative of fresh and deactivated 1/16" 4A molecular sieve obtained from TG/DTA.

From Figures 4.3 and 4.4, there are two derivative peaks for fresh adsorbents which are distinct on the curve at about 61°C and 175°C, implying that the adsorption of water on the 4A molecular sieve occurred in micro-pore and macro-pore. The desorption temperature of both the macro-pore and micro-pore for the 1/16" 4A molecular sieve is lower than for the 1/8" 4A molecular sieve, confirming that the heat can transfer into the small size better than into the big size 4A molecular sieve as mentioned before.

Moreover, the desorption temperature of both adsorbents has trend to shift to the left side or in low temperature direction with the increasing of percentages of the deactivation, as shown in above figures, imply that the adsorption strength of the adsorbents decreases when the degree of deactivation increases. The exact desorption temperatures of both fresh and deactivated 1/8" and 1/16" 4A molecular sieve were obtained from the derivative curves, as shown in Tables 4.3 and 4.4 below.

Table 4.3 Desorption temperature of fresh and deactivated 1/8" 4A molecular sieve at 100%RH and 25°C

% Deactivation	Desorption temperature(°C)	
	Macro-pore	Micro-pore
0	62.5	177
11.36	67.4	168
46.24	64.7	136
53.98	60.9	152
65.42	60.6	134
73.75	60.7	-

Table 4.4 Desorption temperature of fresh and deactivated 1/16" 4A molecular sieve at 100%RH and 25°C

% Deactivation	Desorption temperature(°C)	
	Macro-pore	Micro-pore
0	61.4	172
7.96	60.7	158
62.39	63.3	-
63.96	64.6	-
66.06	62.5	-
82.95	50.7	-

If the amount of water which was adsorbed is compared between micro-pore and macro-pore of the 4A molecular sieve, it is found that most of the water is adsorbed in the micro-pore. The amount of water which adsorbs in the micro-pore and macro-pore vary with the number of batches, as shown in Tables 4.5 and 4.6 below.

Table 4.5 Static adsorption capacities of the 1/8" 4A molecular sieve at 100%RH and 25°C

Number of batches	Adsorption capacity (%wt)	
	Macro-pore	Micro-pore
fresh	7.17	13.93
5	5.66	13.51
15	5.46	7.12
25	4.07	6.89
35	4.22	4.24
45	3.69	2.87

Table 4.6 Static adsorption capacities of the 1/16" 4A molecular sieve at 100%RH and 25°C

Number of batches	Adsorption capacity (%wt)	
	Macro-pore	Micro-pore
fresh	7.22	13.88
5	6.05	13.71
15	9.14	0
25	8.79	0
35	8.33	0
45	4.36	0

4.2 Pressure Drop

From the recent work (Khaikham, 2007), the effect of the pressure drop from the small size of adsorbent was neglected. So, to develop the breakthrough time equation more completely and closer to the real operation than the previous work, the pressure drop was considered. The changing of pressure along with the adsorber was expressed by Ergun's equation:

$$\frac{dP}{dz} = -\frac{G}{\rho g_c D} \left[\frac{1-\varepsilon}{\varepsilon^3} \left[\frac{150(1-\varepsilon)\mu}{D} + 1.75G \right] \right] \quad (4.1)$$

From integrating Equation 4.1, pressure drop was expressed as:

$$P = (2\lambda_0 z + P_0)^{\frac{1}{2}} \quad (4.2)$$

$$\text{where } \lambda_0 = -\frac{G}{\rho_0 g_c D} \left[\frac{1-\varepsilon}{\varepsilon^3} \left[\frac{150(1-\varepsilon)\mu}{D} + 1.75G \right] \right]$$

So, the changing of pressure along with adsorber is shown in Figure 4.5 below.

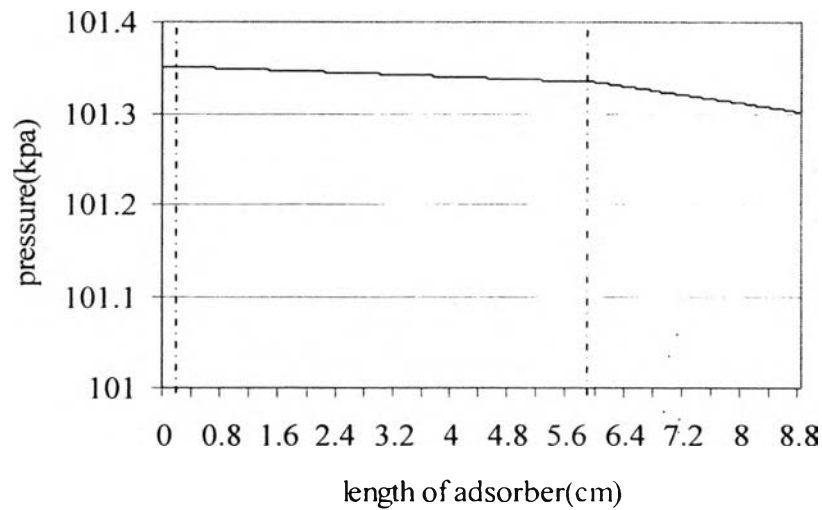


Figure 4.5 Pressure drop along the length of adsorber packed with the fresh adsorbents: 1 atm inlet pressure and 0.00892 m/s superficial velocity.

From Figure 4.5, the adsorber was divided into 3 parts by dash lines that refer to 3 types of adsorbent packed in the adsorber. The last part, which is part of the 1/16" 4A molecular sieve, has the smallest size pellet when compared with the other parts, resulting in the void of the bed becoming small, and making it difficult for the molecules of gas to pass through, affecting the high pressure drop in this zone.

During the experiment under hydrothermal conditions, the adsorbent was destroyed by water and heat, especially at the outer surface of the adsorbent resulting in the size of the pellet decreasing. So, the void fraction that is proportional to the size of the pellet as shown in Appendix C decreased. The void fraction for each type of adsorbent packed in the adsorber changes with the percentage of deactivation, as shown in Figures 4.6, 4.7, and 4.8 below.

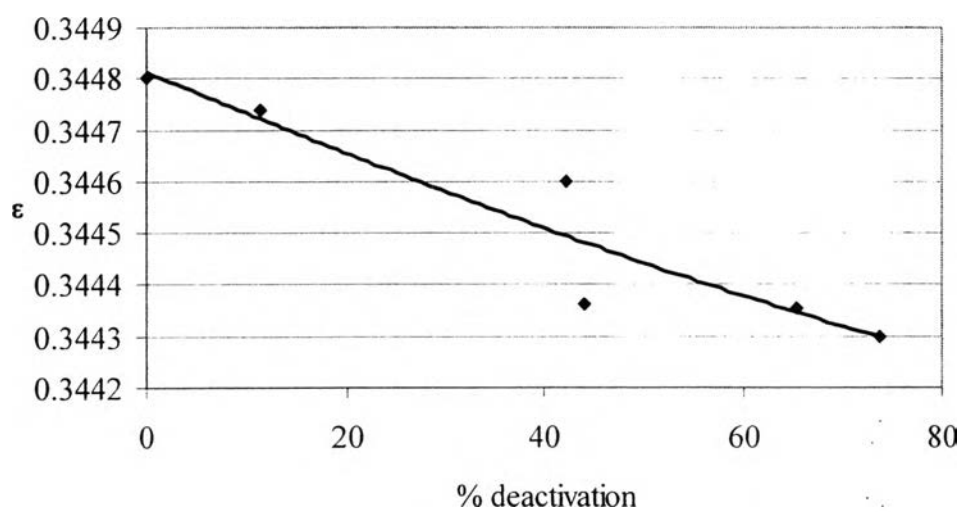


Figure 4.6 Void fraction of 1/8" 4A molecular sieve at various percentages of deactivation.

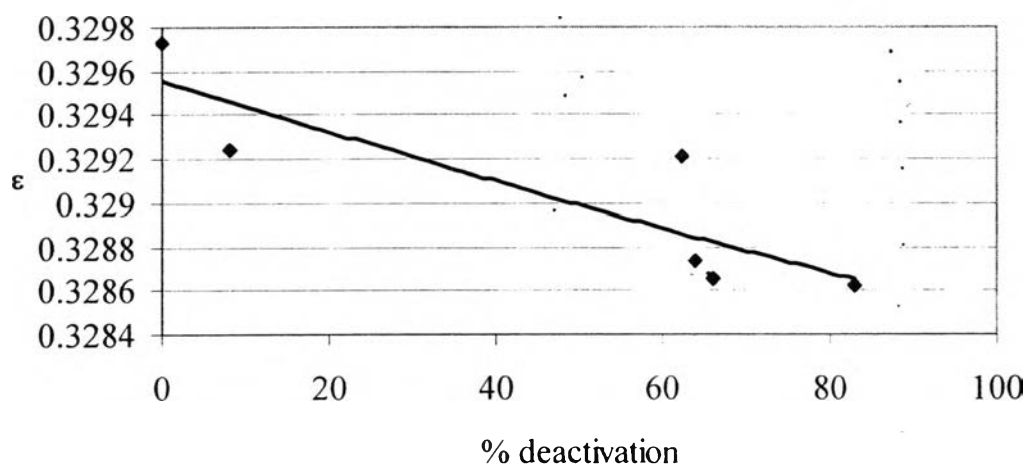


Figure 4.7 Void fraction of 1/16" 4A molecular sieve at various percentages of deactivation.

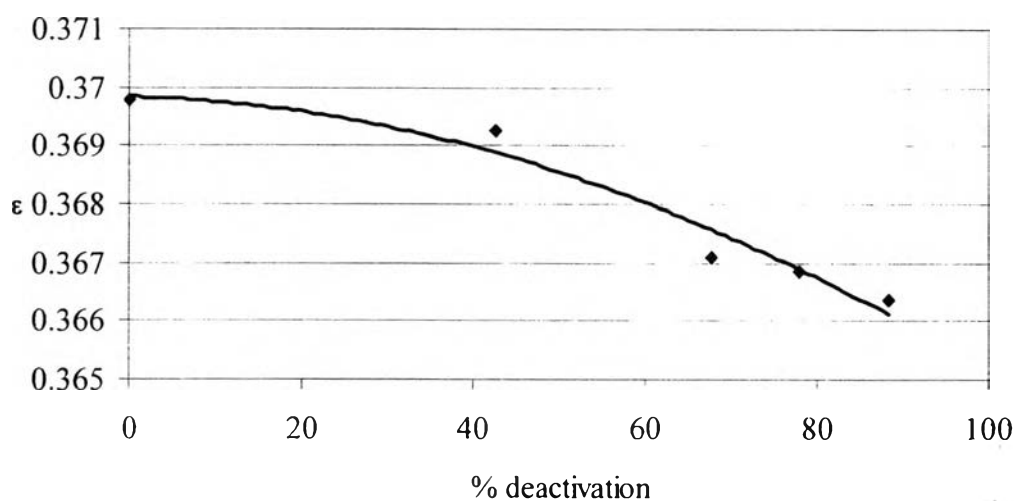


Figure 4.8 Void fraction of activated alumina at various percentages of deactivation.

The decreasing of the void fraction when increasing the percentage of deactivation affects the pressure drop of the deactivated adsorbents which was higher than the fresh adsorbent, as shown in Figure 4.9 below.

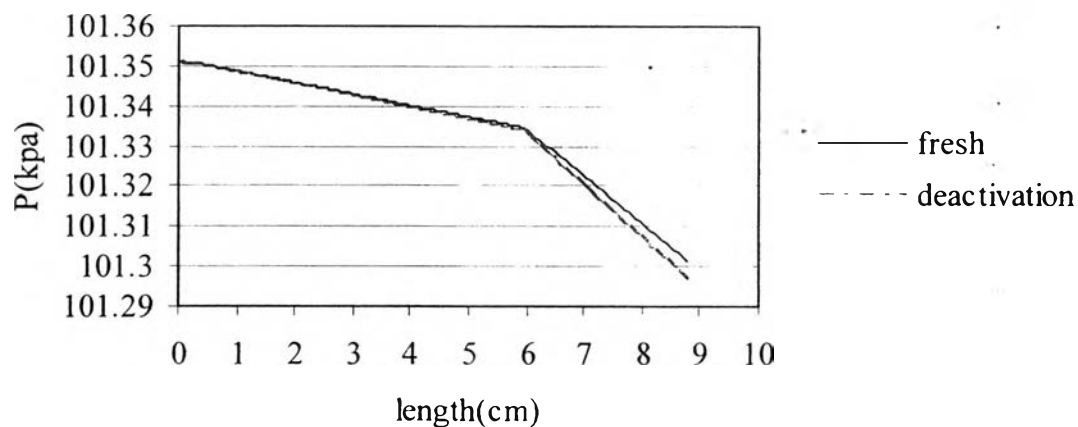


Figure 4.9 Pressure drop along the length of adsorbents packed with the fresh adsorbents and with the highest degree deactivated adsorbents.

The velocity of gas increases along the bed because of the existing pressure drop. The velocity of gas can be written in relation to the pressure drop by assuming steady state and negligible changing in the compressibility:

$$v = \frac{u_0}{(\varepsilon A)(2\lambda_0 z / P_0 + 1)^{\frac{1}{2}}} \quad (4.3)$$

where u_0 is the volume flow rate at inlet.

As mentioned above, when the adsorber was packed with the deactivated adsorbent, the pressure drop was higher than the adsorber packed with the fresh adsorbent resulting in the velocity of gas changing when deactivation occurred, as shown in Figure 4.10 below.

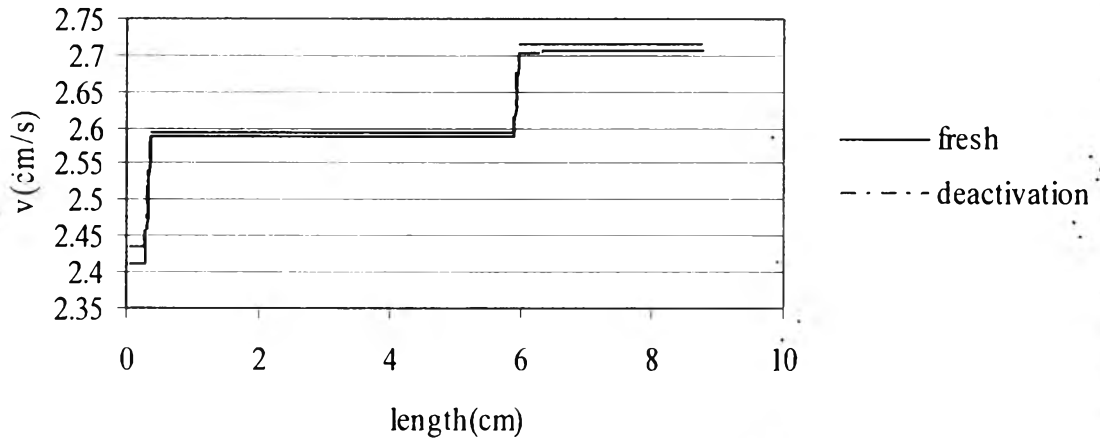


Figure 4.10 Interstitial velocity along the length of adsorber packed with the fresh adsorbents and with the highest degree deactivated adsorbents.

4.3 Estimation of Mass Transfer Coefficient

From the linear driving force (LDF) model, the rate of adsorption can be expressed by the following equation:

$$\frac{\partial \bar{q}}{\partial t} = k(q^* - \bar{q}) \quad (4.4)$$

The LDF mass-transfer coefficient, k , can be related to mass-transfer resistance as follows (Murillo *et al.*, 2004):

$$\frac{1}{k} = \frac{R_p}{3k_f} K + \frac{R_p^2}{15\varepsilon_p D_e} K \quad (4.5)$$

where K and k_f are the equilibrium constant and fluid-phase mass-transfer coefficient, respectively, which were calculated from the following correlation (Murillo *et al.*, 2004):

$$K = \frac{W_0 \rho_b}{C_0} \quad (4.6)$$

and

$$\frac{R_p k_f}{D_m} = 2 + 1.1 \left(\frac{\mu}{\rho D_m} \right)^{\frac{1}{3}} \left(\frac{\rho u R_p}{\mu} \right)^{0.6} \quad (4.7)$$

So, the mass transfer coefficient for each adsorbent was estimated, as shown in Table 4.7 below.

Table 4.7 Overall mass transfer coefficients for each adsorbent and the parameters for calculation of the mass transfer coefficients

	A-201	UI-94 (1/8")	UI-94 (1/16")
Equivalent radius of pellet R_p (m)	0.0016135	0.001542	0.0007955
molecular diffusivity D_m *(m ² /s)	1.77636E-05	1.77636E-05	1.77636E-05
mean pore radius r_p (m)**	1.3E-09	2E-10	2E-10
Tortuosity τ ***	4	3	3
porosity of particle ε_p	0.33	0.32	0.31
D_k *(m ² /s)	5.13082E-05	7.89357E-06	7.89357E-06
effective diffusivity D_e *(m ² /s)	1.08861E-06	5.82941E-07	5.64724E-07
equilibrium constant K	31938.84286	25748.1082	25748.1082
fluid mass-transfer coefficient k_f (m/s)	0.027310532	0.02842832	0.051682138
overall mass transfer coefficient k	6.22684E-05	4.47516E-05	0.000157803

*Appendix D

**Campbell J. M., Gas Conditioning and Processing

***Yang R.T., Gas Aeparation by Adsorption Processes

These overall mass transfer coefficients were different from the previous work in which the mass transfer varies with the type of adsorbents instead of being constant with all three types of adsorbents, as shown in Table 4.8 below.

Table 4.8 Calculated overall mass transfer coefficients compared with those obtained from the previous work

	The overall mass transfer coefficient, k (1/s)			
	This work	Chaikasetpaiboon (2003)	Uttamaroop (2004)	Khaikham (2007)
A-201	6.23×10^{-5}	1.0×10^{-4}	8.5×10^{-5}	8.5×10^{-5}
UI-94 (1/8")	4.48×10^{-5}	1.0×10^{-4}	8.5×10^{-5}	8.5×10^{-5}
UI-94 (1/16")	15.78×10^{-5}	1.0×10^{-4}	8.5×10^{-5}	8.5×10^{-5}

Some parameters which were used to calculate the overall mass transfer coefficient vary when the adsorbents were deactivated, affecting the overall mass transfer coefficient for each type of adsorbent change with the percentage of deactivation, as shown in Tables 4.9, 4.10 and 4.11 below.

Table 4.9 Overall mass transfer coefficients for activated alumina at various percentages of deactivation

A-201	
% Deactivation	Mass transfer coefficient, k (1/s)
0	6.23×10^{-5}
42.46	4.09×10^{-5}
67.92	3.69×10^{-5}

A-201	
% Deactivation	Mass transfer coefficient, k (1/s)
77.97	2.44×10^{-5}
88.3	1.86×10^{-5}

Table 4.10 Overall mass transfer coefficients for 1/ 8" 4A molecular sieve at various percentages of deactivation

1/ 8" 4A molecular sieve	
% Deactivation	Mass transfer coefficient, k (1/s)
0	4.48×10^{-5}
11.36	4.18×10^{-5}
46.24	2.72×10^{-5}
53.98	2.25×10^{-5}
65.42	1.92×10^{-5}
73.75	1.43×10^{-5}

Table 4.11 Overall mass transfer coefficients for 1/ 16" 4A molecular sieve at various percentages of deactivation

1/16" 4A molecular sieve	
% Deactivation	Mass transfer coefficient, k (1/s)
0	15.78×10^{-5}
7.96	14.64×10^{-5}
62.39	7.86×10^{-5}
63.96	7.54×10^{-5}
66.06	7.17×10^{-5}
82.95	3.90×10^{-5}

When the overall mass transfer coefficients decrease, the adsorbents will lose equilibrium capacity and the mass transfer resistance increases because of the difficulty for the water molecule to transfer into the adsorbent pellet, as shown in the above Tables 4.9, 4.10, and 4.11 in which the overall mass transfer coefficients of the three types of adsorbent decrease with the percentage of deactivation.

4.4 Scanning Electron Microscopy of Molecular Sieve Zeolites

Molecular sieve zeolites are crystalline, which are formed by tetrahedras of AlO_4 and SiO_4 . These crystalline structures of Molecular sieve zeolites can be confirmed by Scanning Electron Microscopy (SEM). The SEM images of both fresh 1/8" and 1/16" 4A molecular sieves are shown in Figures 4.11 and 4.12 below.

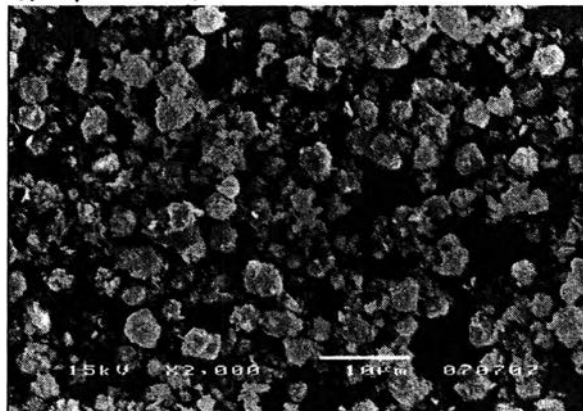


Figure 4.11 Scanning Electron Microscopy image of fresh 1/8" 4A molecular sieve.

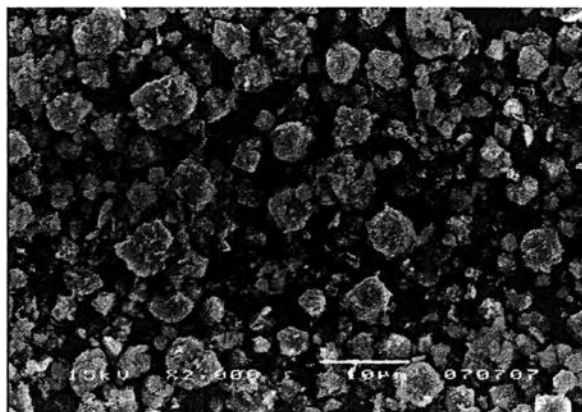
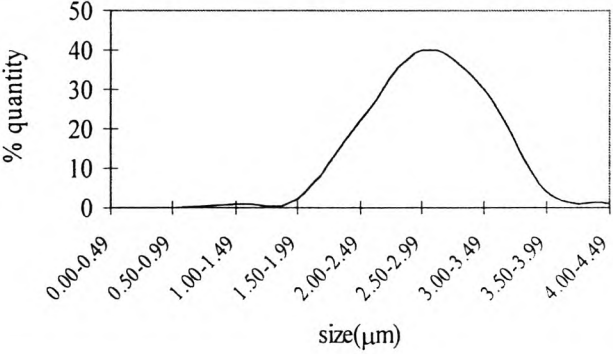
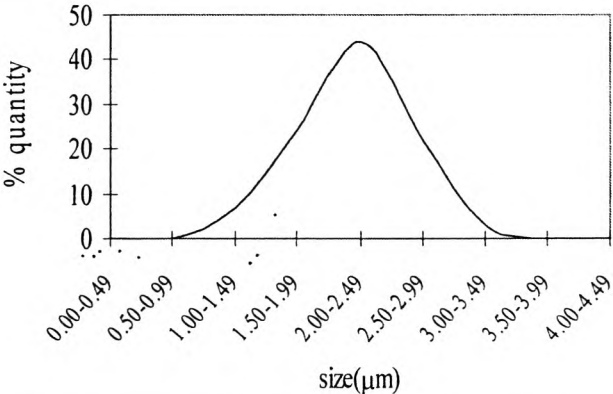
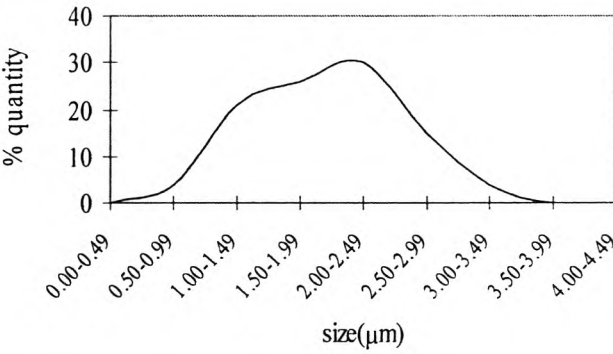
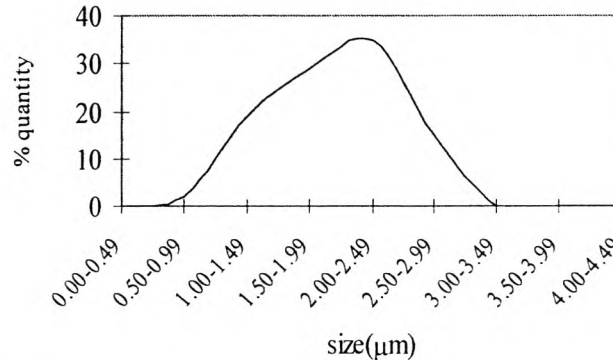


Figure 4.12 Scanning Electron Microscopy image of fresh 1/16" 4A molecular sieve.

The crystal sizes of 1/8" and 1/16" molecular sieve can be decreased because of the hydrothermal conditions during regeneration process, then resulting in the loss of adsorption capacity of adsorbents. Therefore, the degree of deactivation can be determined by the percentage of crystal size reduction. Then, in order to study the changes of crystal size of both adsorbents, SEM was employed to determine the crystal size distribution of 1/8" and 1/16" molecular sieve, as shown in Tables 4.12 and 4.13 below, respectively.

Table 4.12 Crystal size distribution of 1/8" molecular sieve for each degree of deactivation

% Deactivation	Crystal Size Distribution
0	

% Deactivation	Crystal Size Distribution
11.36	
46.24	
53.98	
65.42	

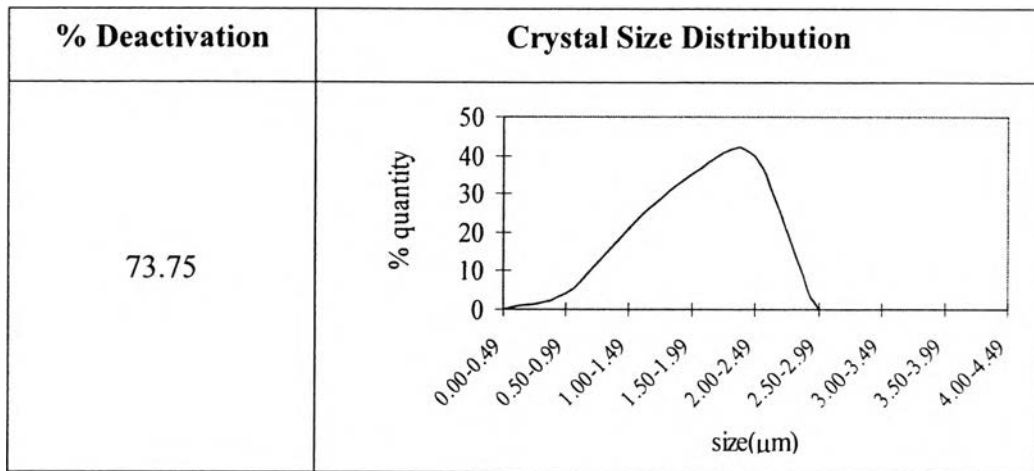
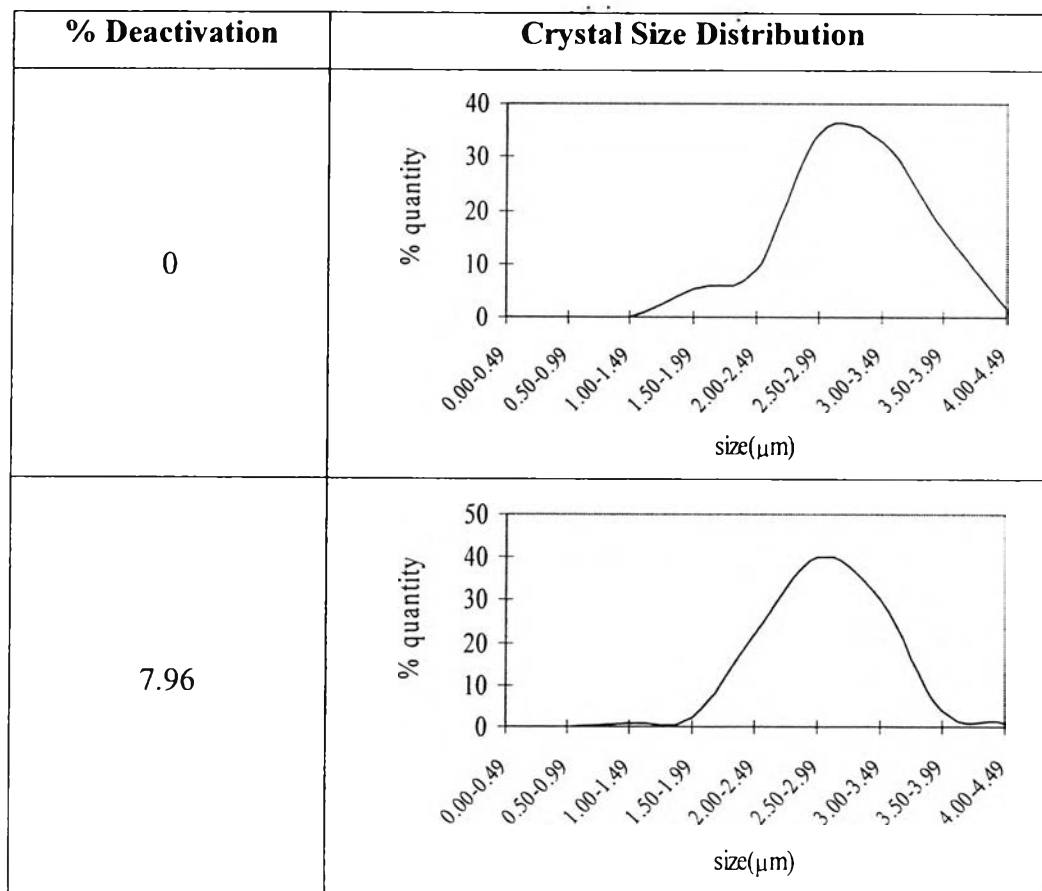
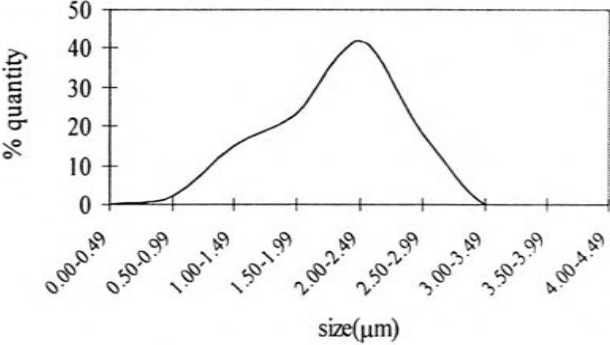
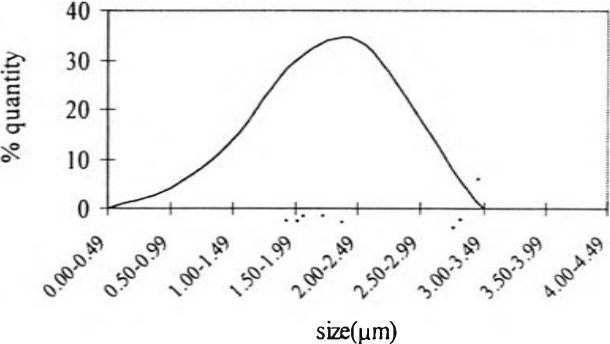
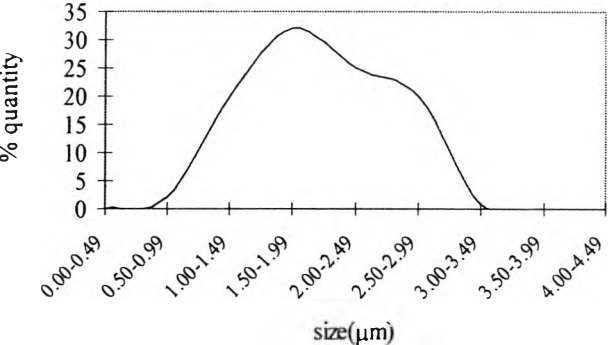
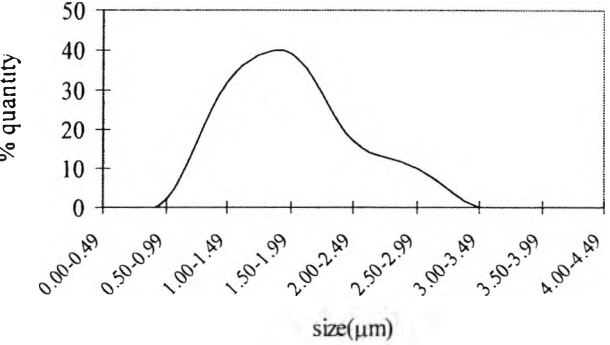


Table 4.13 Crystal size distribution of 1/16" molecular sieve for each degree of deactivation



% Deactivation	Crystal Size Distribution
62.39	
63.96	
66.06	
82.95	

From the above Tables, it is found that peak of size distribution curves shifts to the left hand side or to the small crystal size direction for both 1/8" and 1/16" 4A molecular sieves, which it means that most of the crystals tend to decrease to a small size when the degree of deactivation increases. From the data of crystal size distribution in Appendix B, the decrease of crystal size of both 1/8" and 1/16" 4A molecular sieves can be illustrated by the mean average crystal size, as shown in Table 4.14 below.

Table 4.14 Change of average crystal size of 1/8" and 1/16" 4A molecular sieves with the degrees of deactivation

% Deactivation	UI-94 (1/8")	
	Average crystal size (micron)	% crystal size reduction
0	2.99	0.0
11.36	2.81	6.2
46.24	2.20	26.6
53.98	1.96	34.4
65.42	1.96	34.6
73.75	1.80	39.8
% Deactivation	UI-94 (1/16")	
	Average crystal size (micron)	% crystal size reduction
0	3.00	0.0
7.96	2.82	6.0
62.39	2.04	32.0
63.96	1.99	33.8
66.06	1.97	34.5
82.95	1.75	41.7

The change of the % crystal size reduction for both 1/8" and 1/16" 4A molecular sieves can be related to the % loss of adsorption capacity by the equations; $y = 0.561x$ and $y = 0.516x$, respectively, where x is % average crystal

size reduction and y is % loss of adsorption capacity, as shown in Figures 4.13 and 4.14 below.

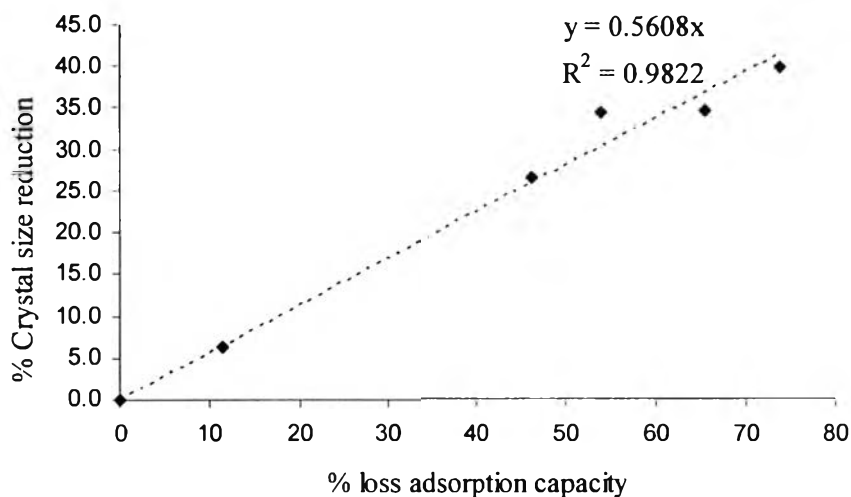


Figure 4.13 The loss of adsorption capacity of 1/8" molecular sieve as a function of the crystal size reduction.

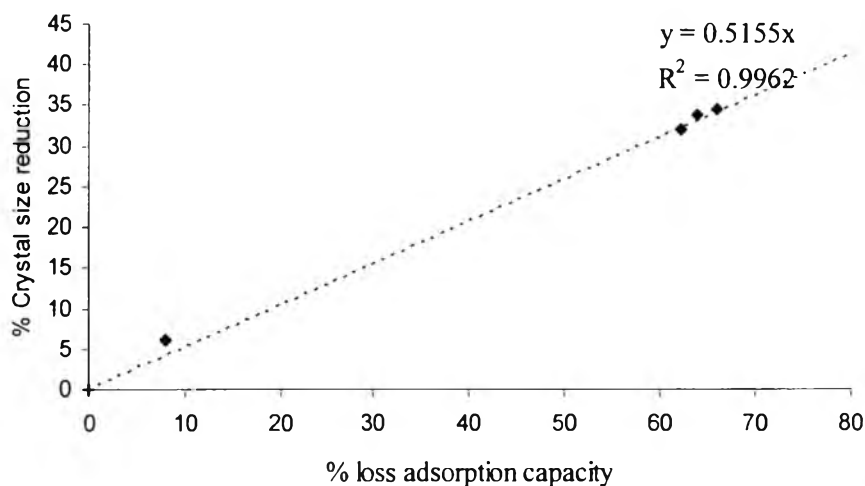


Figure 4.14 The loss of adsorption capacity of 1/16" molecular sieve as a function of the crystal size reduction.

From the above figures, it is found that when the crystal size reduction increases, the loss in adsorption capacity increases. It can be explained that the breakdown of crystal size of both 1/8" and 1/16" 4A molecular sieves has the effect to the loss of adsorption capacity.

4.5 Equilibrium Adsorption Isotherms

The equilibrium adsorption isotherms of water for both sizes of adsorbent, 1/8" and 1/16" 4A molecular sieves were determined on both fresh and deactivated adsorbents. In this work, the equilibrium adsorption isotherms of each adsorbent were investigated as in the Uttamaroop's work, and the relative humidity was varied between 2 to 75%. In order to describe the adsorption isotherms, the standard adsorption isotherms were applied to fit with the data from the experiments. Moreover, many of them were shown to be the best models, which fit well with the experimental data.

4.5.1 The Equilibrium Adsorption Isotherm of Fresh Adsorbents

From the previous work (Khaikham, 2007), the adsorption isotherms of fresh 4A molecular sieve of both sizes fit well with the standard isotherm Type II, which was classified by Brunauer, as shown in Figures 4.15 and 4.16. It means that the adsorbent adsorbs water vapor firstly with the monolayer, and then the multilayers occur because water is saturated in the pore. The adsorption isotherm from the experiment shows that the 4A molecular sieve zeolite has high adsorption capacity at low relative humidity. That is the reason why the 4A molecular sieve zeolite was packed at the lower zone guarded with alumina on top. When wet gas passes through the alumina zone, the relative humidity decreased to lower relative humidity that is suitable for 4A molecular sieve zeolite.

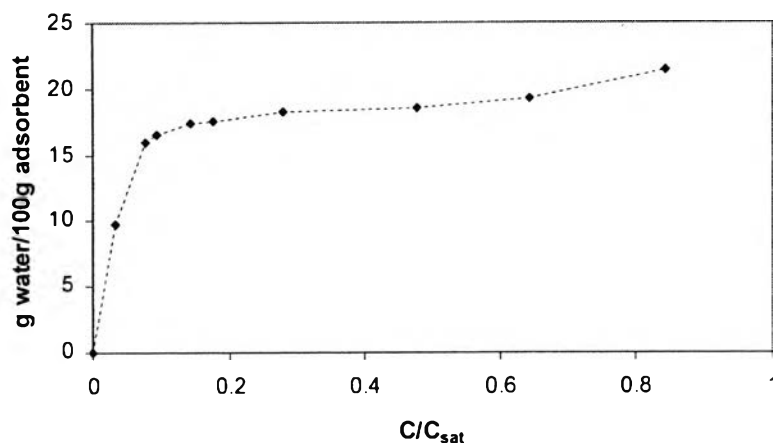


Figure 4.15 Langmuir adsorption isotherm of fresh 1/8" 4A molecular sieve zeolite (Khaikham, 2007).

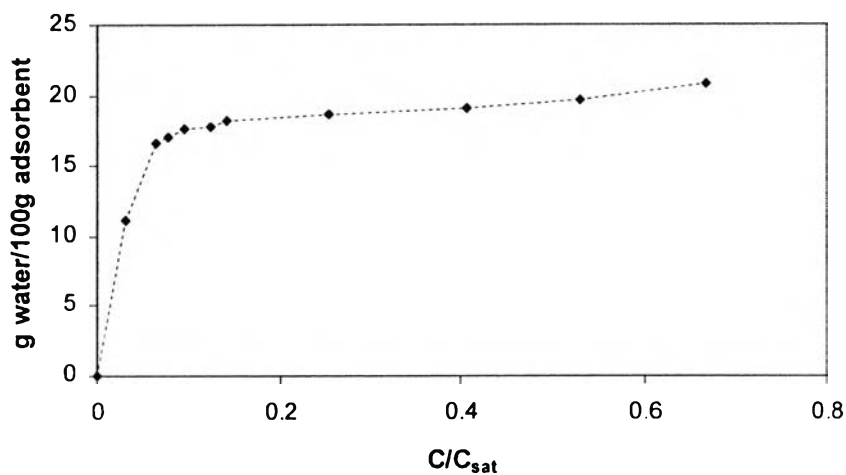


Figure 4.16 Langmuir adsorption isotherm of fresh 1/16" 4A molecular sieve zeolite (Khaikham, 2007).

The adsorption isotherm models including the Slips, UNILAN, Toth, Langmuir, A-D for Toth, A-D for Slips, A-D for UNILAN, and A-D for Langmuir model used for explanation of the adsorption behavior of monolayer and multilayer were compared in order to select the best models that fit with the adsorption isotherm data of both fresh 1/8" and 1/16" molecular sieves from the experiments, as shown in Figures 4.17-4.20 below.

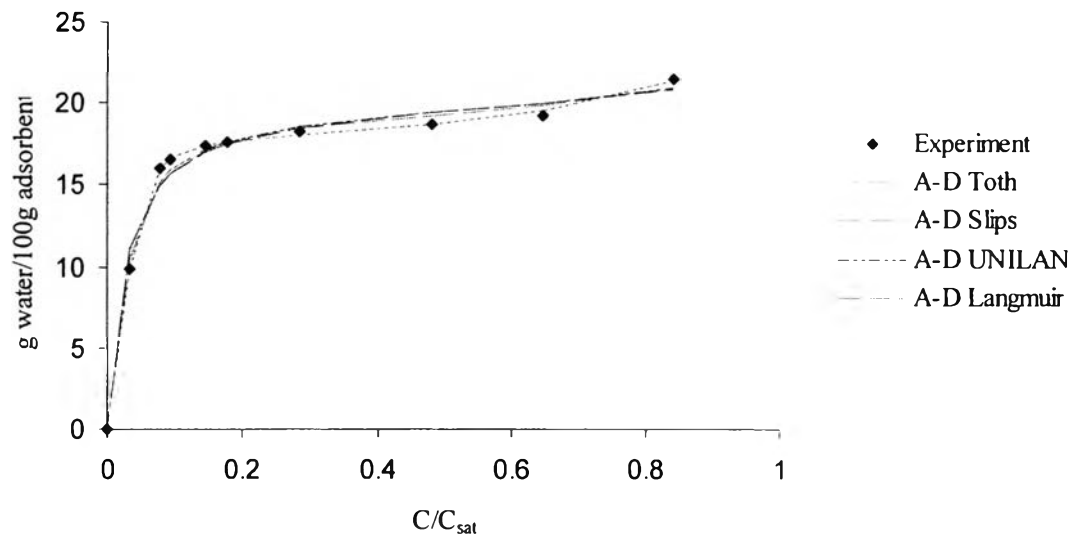


Figure 4.17 Comparison of model predictions with the experimental data for fresh 1/8" 4A molecular sieve.

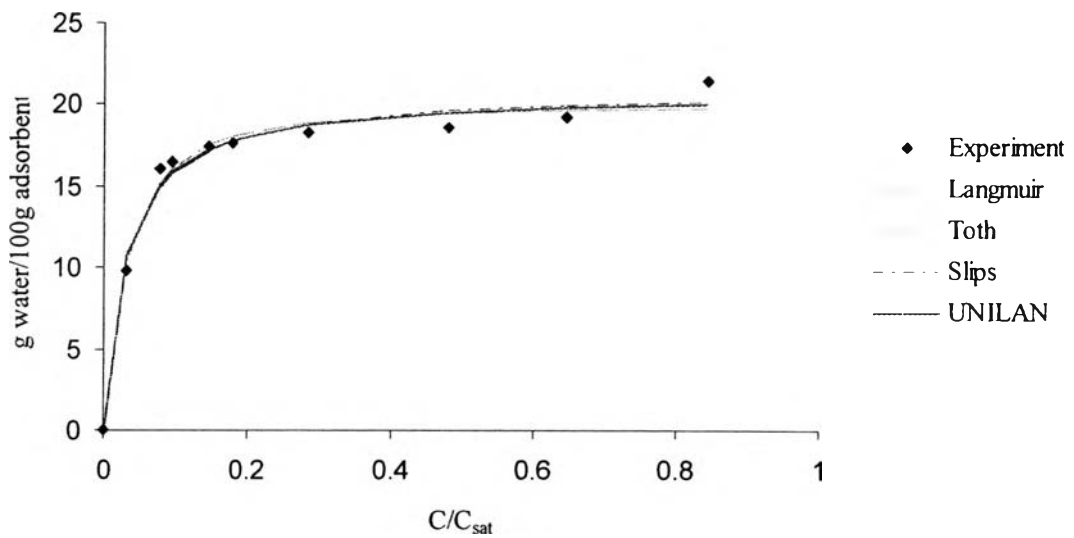


Figure 4.18 Comparison of model predictions with the experimental data for fresh 1/8" 4A molecular sieve.

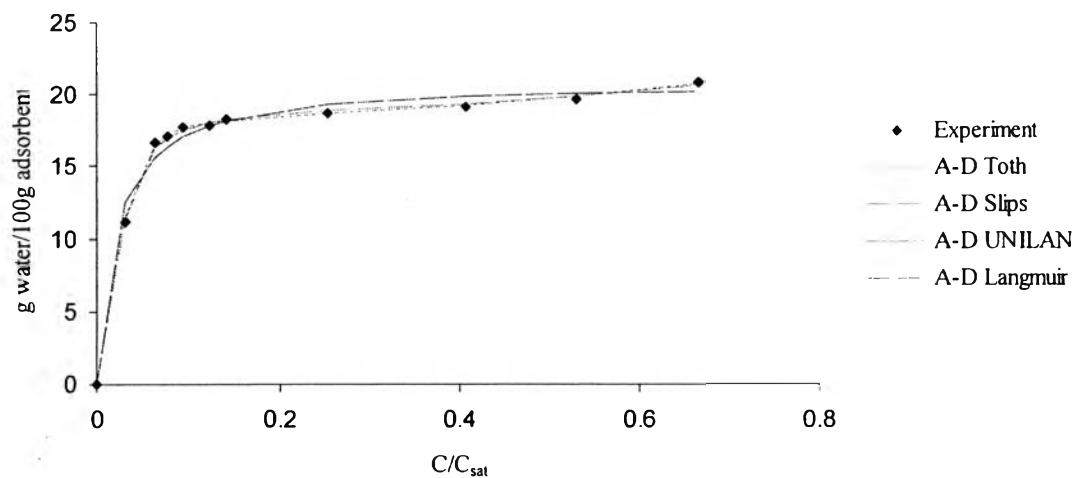


Figure 4.19 Comparison of model predictions with the experimental data for fresh 1/16" 4A molecular sieve.

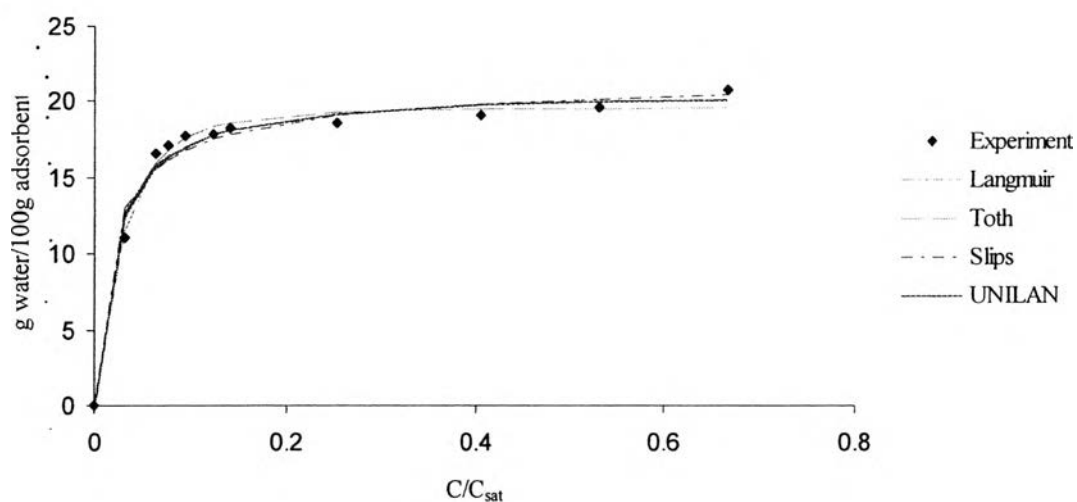


Figure 4.20 Comparison of model predictions with the experimental data for fresh 1/16" 4A molecular sieve.

From the above figures, most of adsorption isotherm equations can be fitted with the experimental data. To determine the best fit, the r^2 of every model is shown in Tables 4.15 and 4.16 below.

Table 4.15 Comparison of r^2 for each model for fresh 1/8" molecular sieve

Models	Adsorption isotherm equation	r^2
A-D Slips	$q = \frac{2543.57C_r^{1.36}}{(1 + (37.28C_r)^{1.36})(1 - C_r)^{0.06}}$	0.993
A-D UNILAN	$q = \frac{1}{8.45 \times 10^{-5} (1 - C_r)^{0.04}} \ln\left(\frac{1 + 39.75C_r e^{8.39 \times 10^{-4}}}{1 + 39.75C_r e^{-8.39 \times 10^{-4}}}\right)$	0.985
A-D Langmuir	$q = \frac{789.07C_r}{(1 + 39.75C_r)(1 - C_r)^{0.04}}$	0.985
A-D Toth	$q = \frac{328.13C_r}{(1 + (18.75C_r)^{2.90})^{\frac{1}{2.90}} (1 - C_r)^{0.10}}$	0.999
Slips	$q = \frac{594.10C_r^{0.95}}{(1 + (34.01C_r)^{0.95})}$	0.981
UNILAN	$q = \frac{1}{8.81 \times 10^{-5}} \ln\left(\frac{1 + 34.14C_r e^{9.12 \times 10^{-4}}}{1 + 34.14C_r e^{-9.12 \times 10^{-4}}}\right)$	0.982
Langmuir	$q = \frac{708.34C_r}{(1 + 34.14C_r)}$	0.982
Toth	$q = \frac{19.93C_r}{(0.01 + C_r^{1.37})^{\frac{1}{1.37}}}$	0.984

Table 4.16 Comparison of r^2 for each model for fresh 1/16" molecular sieve

Models	Adsorption isotherm equation	r^2
A-D Slips	$q = \frac{4.54 \times 10^4 C_r^{2.13}}{(1 + (38.92C_r)^{2.13})(1 - C_r)^{0.1}}$	0.998
A-D UNILAN	$q = \frac{1}{-2.14 \times 10^{-4} (1 - C_r)^{-0.01}} \ln\left(\frac{1 + 46.42C_r e^{-0.002}}{1 + 46.42C_r e^{0.002}}\right)$	0.984
A-D Langmuir	$q = \frac{971.94C_r}{(1 + 46.42C_r)(1 - C_r)^{-0.01}}$	0.984

Models	Adsorption isotherm equation	r ²
A-D Toth	$q = \frac{361.57C_r}{(1 + (20.37)^{1.65})^{\frac{1}{1.65}} (1 - C_r)^{0.23}}$	1.000
Slips	$q = \frac{425.19C_r^{0.75}}{(1 + (52.23C_r)^{0.75})}$	0.977
UNILAN	$q = \frac{1}{3 \times 10^{-5}} \ln\left(\frac{1 + 47.26C_r e^{3.13 \times 10^{-4}}}{1 + 47.26C_r e^{-3.13 \times 10^{-4}}}\right)$	0.984
Langmuir	$q = \frac{984.77C_r}{(1 + 47.26C_r)}$	0.984
Toth	$q = \frac{19.66C_r}{(0.003 + C_r^{1.86})^{\frac{1}{1.86}}}$	0.991

From the above tables, it was found that almost all of models of multilayer adsorption isotherms fit with the experimental data better than model of monolayer adsorption isotherms, especially the A-D for Toth Model that shows the best fit with the experimental data for both size of 4A molecular sieve. This is because they can explain an adsorption isotherm for both monolayer and multilayer part, which is different from the models of monolayer adsorption isotherm limited for the adsorption only in monolayer form. So, at the high relative humidity, when the multilayers occur, the latter models can not explain the behavior of adsorption. However, the models of monolayer adsorption isotherm well fit with the experimental data as shown in above tables because the curve of the adsorption isotherm of fresh 4A molecular sieve is so closed to the monolayer adsorption isotherm form.

4.5.2 Deactivated Molecular Sieve Zeolite

The adsorption isotherm of deactivated zeolites was investigated for being used in the prediction of the breakthrough time for many cases of deactivation. The adsorption isotherms show that the static adsorption of adsorbent fast decreases with the number of batches, especially from fresh to 15 batches (about 54%

deactivation). After that the static adsorption isotherm slightly changes, which means that the adsorption ability of adsorbent does not change much when the number of batches (or the degree of deactivation) increases as shown in Figures 4.21 and 4.22 below.

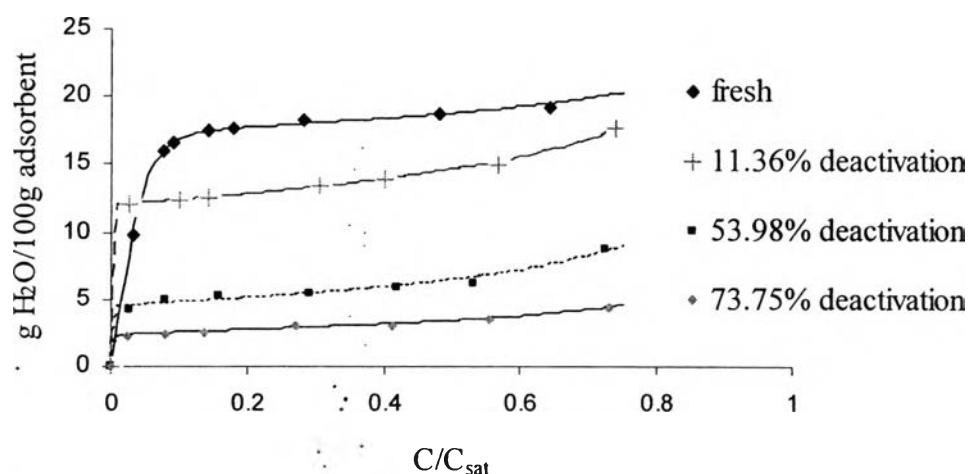


Figure 4.21 Adsorption isotherms of 1/8" 4A molecular sieve at each degree of deactivation.

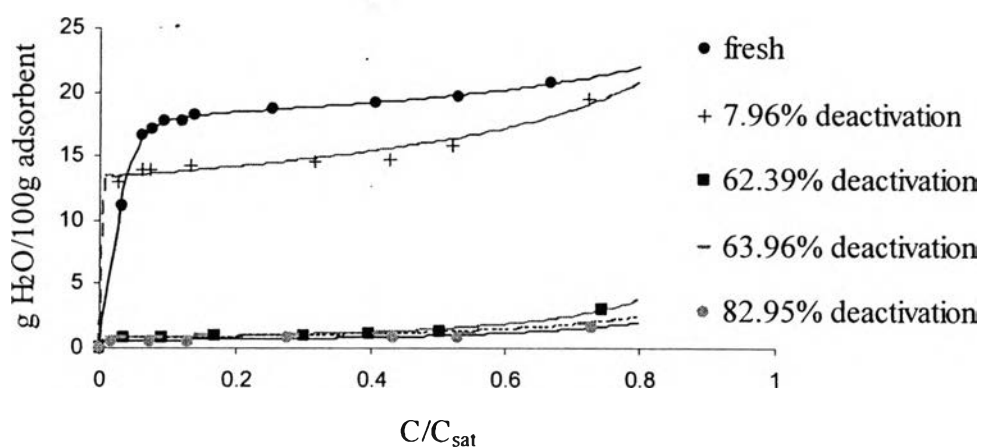


Figure 4.22 Adsorption isotherms of 1/16" 4A molecular sieve at each degree of deactivation.

From the above figures, the curves of adsorption isotherm for 1/16" 4A molecular sieves become flat faster than the curves of 1/8" 4A molecular sieves when deactivation occurs. This is because the smaller size can be destroyed more easily than the bigger size as mentioned before. Moreover, after the deactivation occurs, the curve of adsorption isotherm changes in such a way that the multilayer adsorption occurs immediately as compared to the adsorption isotherms from 4A molecular sieves at the lower degrees of deactivation. As a result, the Slips, UNILAN, Toth, and Langmuir model used to explain monolayer adsorption isotherm do not well fit with the experimental data as shown in Tables 4.17 and 4.18, which r^2 tends to decrease with the degree of deactivation more than the other model.

Table 4.17 Change of r^2 of each model for 1 /8" 4A molecular sieve at various degrees of deactivation

		Degree of deactivation				
		Fresh	11.63%	46.24%	53.98%	73.75%
	A-D Toth	0.999	0.997	0.991	0.979	0.997
	A-D Slips	0.999	0.997	0.990	0.987	0.997
	A-D Unilan	0.962	0.996	0.990	0.985	0.996
r^2	A-D Langmuir	0.967	0.997	0.993	0.972	0.997
	Langmuir	0.888	0.813	0.627	0.691	0.519
	Toth	0.891	0.814	0.627	0.946	0.522
	Slips	0.942	0.813	0.627	0.893	0.522
	UNILAN	0.982	0.961	0.916	0.891	0.925

*Appendix E

Table 4.18 Change of r^2 of each model for 1 /16" 4A molecular sieve at various degrees of deactivation

		Degree of deactivation				
		Fresh	7.96%	62.39%	63.96%	82.95%
r^2	A-D Toth	1.000	0.987	0.952	0.980	0.981
	A-D Slips	1.000	0.989	0.974	0.858	0.980
	A-D Unilan	0.960	0.988	0.974	0.980	0.981

		Degree of deactivation				
		Fresh	7.96%	62.39%	63.96%	82.95%
r^2	A-D Langmuir	0.968	0.989	0.925	0.979	0.978
	Langmuir	0.895	0.840	0.634	0.702	0.065
	Toth	0.955	0.840	0.159	0.418	0.655
	Slips	0.955	0.843	0.164	0.799	0.717
	UNILAN	0.984	0.948	0.708	0.779	0.745

*Appendix E

From the above tables, when the deactivation occurs, it is found that A-D for Toth is not the best fit model with the experimental data as in the case of fresh adsorbent. However, even through the A-D for Toth is not the best fit with the experimental data for all degrees of deactivation, it is selected to explain the adsorption isotherm because the r^2 is not much different with the best fit model. The A-D for Toth model for each degree of deactivation is shown in Tables 4.19 and 4.20 below.

Table 4.19 The A-D for Toth model for 1/8" 4A molecular sieve at each degree of deactivation

%Deactivation	Equilibrium adsorption isotherm equation *	r^2
fresh	$\frac{q}{q_m} = \frac{18.75C_r}{(1 + (18.75C_r)^{2.90})^{\frac{1}{2.90}} (1 - C_r)^{0.10}}$	0.999
11.36%	$\frac{q}{q_m} = \frac{213.09C_r}{(1 + (213.09C_r)^{1.40})^{\frac{1}{1.40}} (1 - C_r)^{0.24}}$	0.997
46.24%	$\frac{q}{q_m} = \frac{280.76C_r^{1.20}}{(1 + (280.76C_r)^{1.20})(1 - C_r)^{0.37}}$	0.991
53.98%	$\frac{q}{q_m} = \frac{394.90C_r}{(1 + (394.90C_r)^{0.67})^{\frac{1}{0.67}} (1 - C_r)^{0.36}}$	0.979

%Deactivation	Equilibrium adsorption isotherm equation*	r ²
73.75%	$\frac{q}{q_m} = \frac{400.95C_r}{(1 + (400.95C_r)^{1.02})^{\frac{1}{1.02}} (1 - C_r)^{0.44}}$	0.997

* C_r = concentration of vapor water in natural gas/ saturated concentration of vapor water in natural gas

Table 4.20 The A-D for Toth model for 1/16" 4A molecular sieve at each degree of Deactivation

%Deactivation	Equilibrium adsorption isotherm equation*	r ²
fresh	$\frac{q}{q_m} = \frac{20.37C_r}{(1 + (20.37C_r)^{1.65})^{\frac{1}{1.65}} (1 - C_r)^{0.23}}$	1.000
7.96%	$\frac{q}{q_m} = \frac{102.00C_r}{(1 + (102.00C_r)^{1.65})^{\frac{1}{1.65}} (1 - C_r)^{0.23}}$	0.987
62.39%	$\frac{q}{q_m} = \frac{314.10C_r}{(1 + (314.10C_r)^{0.48})^{\frac{1}{0.48}} (1 - C_r)^{0.89}}$	0.952
63.96%	$\frac{q}{q_m} = \frac{344.40C_r}{(1 + (344.40C_r)^{1.17})^{\frac{1}{1.17}} (1 - C_r)^{0.67}}$	0.980
82.95%	$\frac{q}{q_m} = \frac{415.09C_r}{(1 + (415.09C_r)^{1.02})^{\frac{1}{1.02}} (1 - C_r)^{0.88}}$	0.981

* C_r = concentration of vapor water in natural gas/ saturated concentration of vapor water in natural gas

4.6 The Change of Parameters in Adsorption Isotherms Model the Degree of Deactivation

The adsorption isotherm model that was proposed by Aranovich and Donohue is $a(p) = f(c)/(1 - c/c_s)^d$. Function $f(c)$ describes the adsorption isotherm in the first monolayer, which in this work the Toth model was chosen, and the term $1/(1 - c/c_s)^d$ describes the adsorption in the subsequent layers. The parameters in this model were determined by fitting the model with the experimental data. The results are shown in Table 4.21 below.

Table 4.21 Values of all parameters in the A-D for Toth equation at each degree of deactivation

Adsorbent	%deactivation	Parameters			
		A-D for Toth ($q = q_m(bC_r)/((1+(bC_r)^t)^{1/t}(1-C_r)^d)$)			
		qm	b	t	d
1/8" Molsiv	0	17.50	18.75	2.90	0.10
	11.36	12.44	213.09	1.40	0.24
	46.24	5.65	280.76	1.20	0.37
	53.98	5.38	394.90	0.67	0.36
	73.75	2.46	400.95	1.02	0.44
1/16" Molsiv	0	17.75	20.37	3.88	0.14
	7.96	13.95	102.00	1.65	0.23
	62.39	0.97	314.10	0.48	0.89
	63.96	0.79	344.40	1.17	0.67
	82.95	0.53	415.09	1.02	0.88

From the above table, the parameters change with the degree of deactivation, so if parameters are plotted against the degree of deactivation, then adsorption isotherm at any percentage of deactivation can be predicted. The relationship between each parameter with the degree of deactivation is shown in Figures 4.23 to 4.27 below.

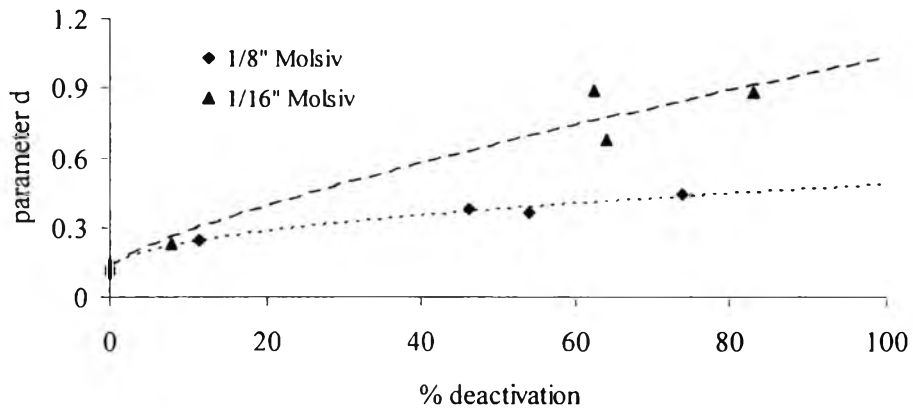


Figure 4.23 Relationship between the parameter “d” in the A-D for Toth equations For the 1/8" and 1/16" molecular sieve zeolite and the degree of deactivation.

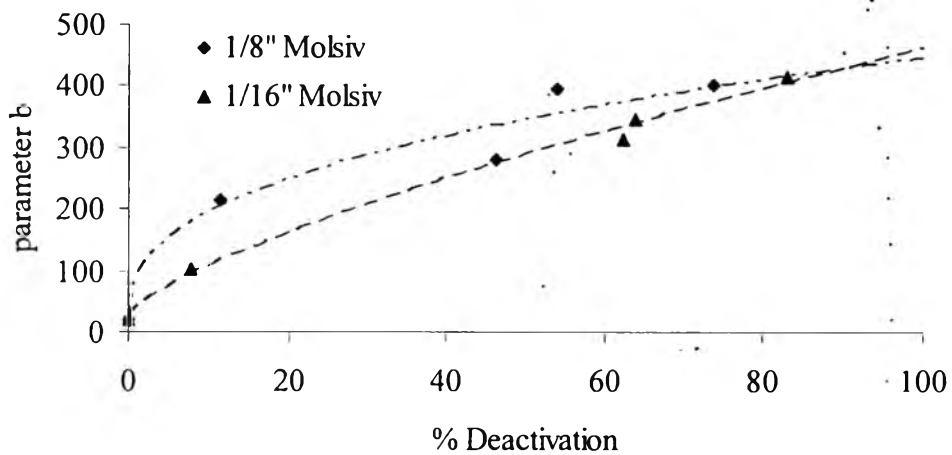


Figure 4.24 Relationship between the parameter “b” in the A-D for Toth equations for the 1/8" and 1/16" molecular sieve zeolite and the degree of deactivation.

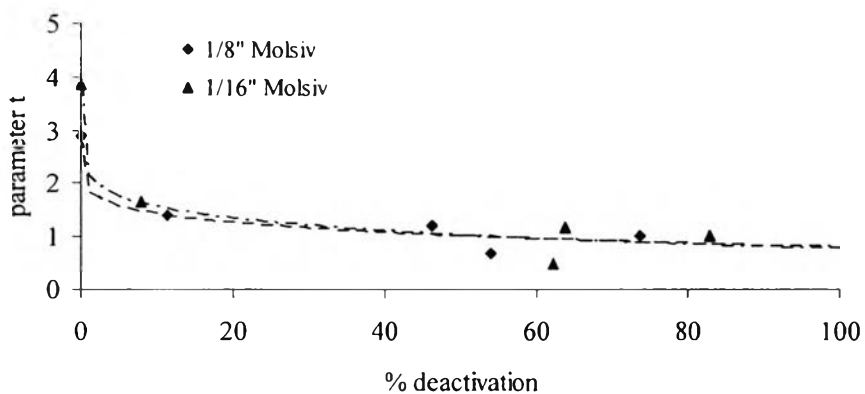


Figure 4.25 Relationship between the parameter “t” in the A-D for Toth equations for the 1/8" and 1/16" molecular sieve zeolite and the degree of deactivation.

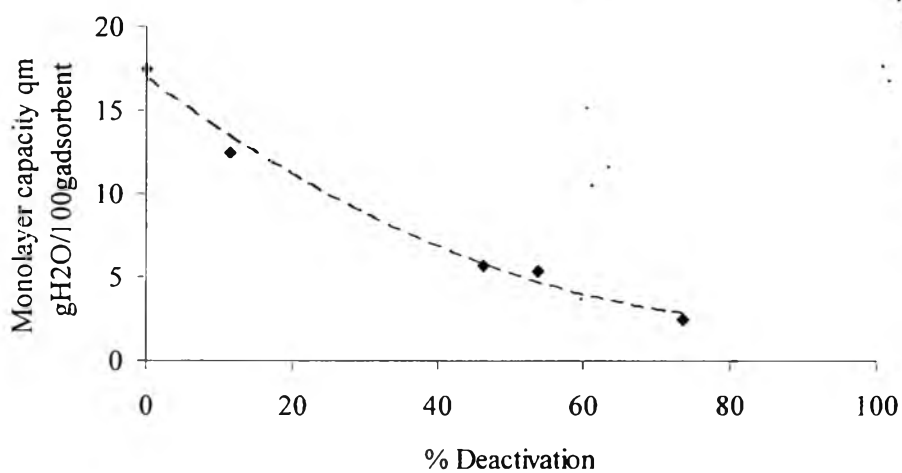


Figure 4.26 Relationship between the monolayer capacity of the 1/8" molecular sieve zeolite and the degree of deactivation.

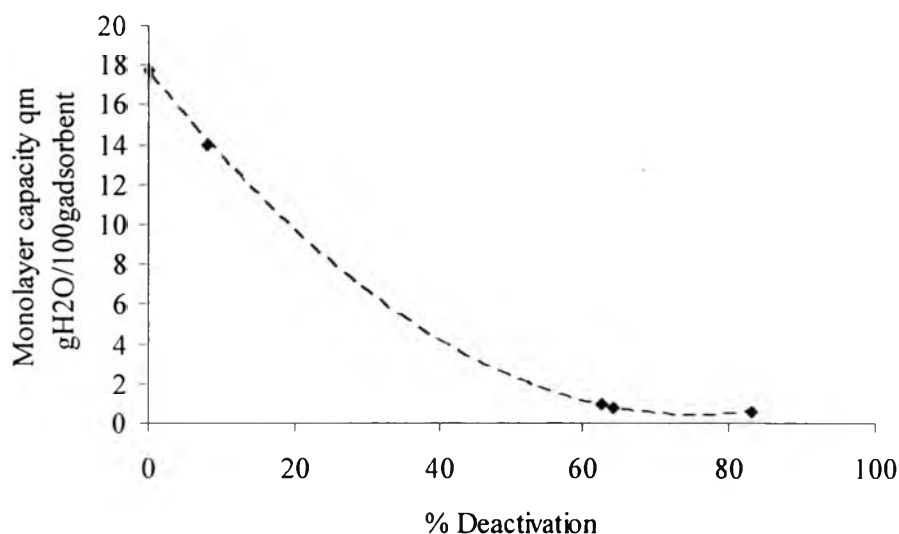


Figure 4.27 Relationship between the monolayer capacity of the 1/6" molecular sieve zeolite and the degree of deactivation.

From above Figures, the plots show the increase of parameter "d" with the degree of deactivation, and because the term $(1 - c_r)$ is less than 1, so the increase of "d" then makes the term $(1 - c_r)^d$ smaller, or the term $1/(1 - c_r)^d$ becomes larger. Therefore, the increase of "d" refers to the multilayer occurs immediately. Additionally, the parameters "b" and "q_m" decrease, but the parameter "t" increases with the degree of deactivation. Since it quite complicates to explain each parameter separately, the whole of term $qm(bc_r)/(1 - (bc_r)^t)$ was therefore considered. It was found that the change of those parameters made this term smaller. Thus, the adsorption isotherms get more flat with the degree of deactivation. To predict the adsorption isotherm changing with the degree of deactivation, all of parameters were fitted to a function at each degree of deactivation as shown in Tables 4.22 and 4.23 below.

Table 4.22 Parameters in the A-D for Toth equations of the 1/8" molecular sieve zeolite as a function of the degree of deactivation

1/8" Molsiv	
Equations	r ²
$b(D) = 70.88D^{0.389} + 20.024$	0.953
$d(D) = 0.043D^{0.472} + 0.105$	0.991
$t(D) = -1.039D^{0.154} + 2.903$	0.951
$q_m(D) = -1.270D^{0.574} + 17.510$	0.998

*D = Degree of deactivation

Table 4.23 Parameters in the A-D for Toth equations of the 1/16" molecular sieve zeolite as a function of the degree of deactivation

1/16" Molsiv	
Equations	r ²
$b(D) = 15.513D^{0.724} + 24.188$	0.995
$d(D) = 0.026D^{0.768} + 0.126$	0.942
$t(D) = -1.740D^{0.126} + 3.877$	0.957
$q_m(D) = -1.442D^{0.583} + 18.028$	0.983

*D = Degree of deactivation

So, if the parameters in the above tables were substituted in the A-D for Toth equation, the adsorption isotherm for the 4A molecular sieve of both sizes at any degree of deactivation can be predicted by:

$$q(D) = \frac{q_m(D)b(D)C_r}{(1 + (b(D)C_r)^{t(D)})^{\frac{1}{d(D)}} (1 - C_r)^{d(D)}} \quad (4.8)$$

Similarly, from the previous work, the adsorption isotherm of alumina can be explained by Freundlich isotherm, $q = ac^b$ (Khaikham, 2007). The parameter "a" and "b" in the Freundlich model can be shown in the relationship with the degree of deactivation as shown in Figures 4.28 and 4.29 below.

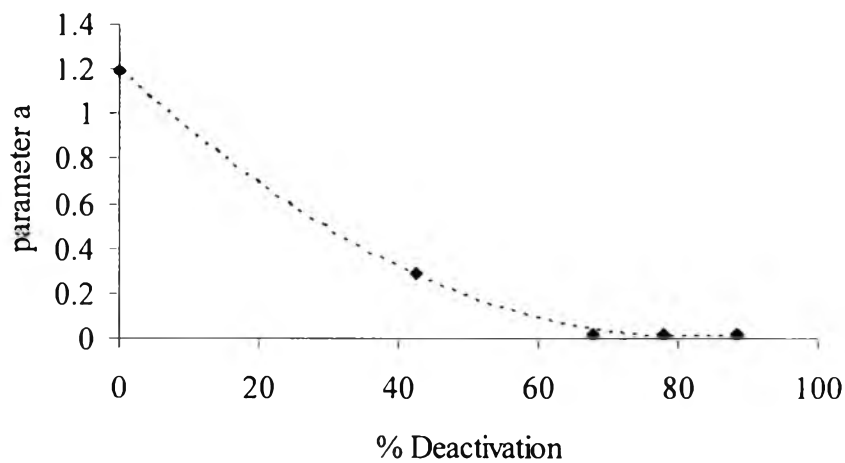


Figure 4.28 Relationship between the parameter “a” in Freundlich equations for the alumina adsorbent and the degree of deactivation.

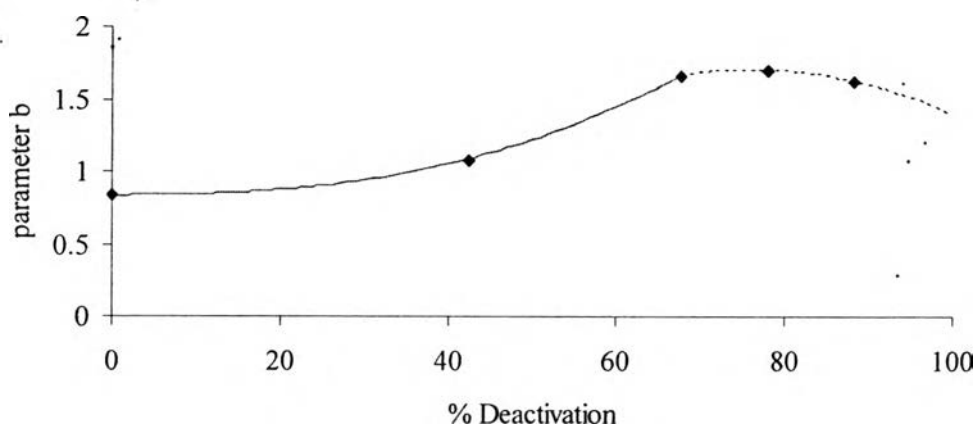


Figure 4.29 Relationship between the parameter “b” in Freundlich equations for the alumina adsorbent and the degree of deactivation.

From the above graphs, the parameters can be written as a function of the degree of deactivation as shown in Table 4.24

Table 4.24 Parameters in the Freundlich equations of the Alumina as a function of the degree of deactivation

Alumina	
Equations	r^2
$a(D) = 0.0002D^2 - 0.0291D + 1.1971$	0.999
$b(D) = 2.09 \times 10^{-5} D^{2.510} + 0.829; 0 \leq D \leq 67.9$	1.000
$b(D) = -5.461 \times 10^{-4} D^2 + 0.083D - 1.487; 67.9 \leq D \leq 100$	0.957

Thus, the adsorption isotherm of alumina written as a function of the degree of deactivation is:

$$q(D) = a(D)c^{b(D)} \quad (4.9)$$

From Equations 4.8 and 4.9, the adsorption isotherm for each degree of deactivation was predicted as shown in Tables 4.25-4.27 below.

Table 4.25 The predicted adsorption isotherms for 1/8" molecular sieve zeolite at various degrees of deactivation

1/8" Molsiv	
% Deactivation	Predicted Isotherm
5	$\frac{q}{q_m} = \frac{152.531C_r}{(1 + 152.531C_r)^{1.572} \frac{1}{1.572} (1 - C_r)^{0.196}}$
10	$\frac{q}{q_m} = \frac{193.512C_r}{(1 + 193.512C_r)^{1.421} \frac{1}{1.421} (1 - C_r)^{0.231}}$
15	$\frac{q}{q_m} = \frac{223.133C_r}{(1 + 223.133C_r)^{1.326} \frac{1}{1.326} (1 - C_r)^{0.258}}$
20	$\frac{q}{q_m} = \frac{247.169C_r}{(1 + 247.169C_r)^{1.254} \frac{1}{1.254} (1 - C_r)^{0.280}}$
25	$\frac{q}{q_m} = \frac{267.754C_r}{(1 + 267.75C_r)^{1.197} \frac{1}{1.197} (1 - C_r)^{0.299}}$

1/8" Molsiv	
% Deactivation	Predicted Isotherm
30	$\frac{q}{q_m} = \frac{285.951C_r}{(1 + 285.951C_r)^{1.148} \frac{1}{1.197} (1 - C_r)^{0.317}}$
35	$\frac{q}{q_m} = \frac{302.375C_r}{(1 + 302.375C_r)^{1.106} \frac{1}{1.106} (1 - C_r)^{0.333}}$
40	$\frac{q}{q_m} = \frac{317.419C_r}{(1 + 317.419C_r)^{1.068} \frac{1}{1.068} (1 - C_r)^{0.348}}$

Table 4.26 The predicted adsorption isotherms for 1/16" molecular sieve zeolite at various degrees of deactivation

1/16" Molsiv	
% Deactivation	Equations
5	$\frac{q}{q_m} = \frac{73.953C_r}{(1 + 73.953C_r)^{1.744} \frac{1}{1.744} (1 - C_r)^{0.216}}$
10	$\frac{q}{q_m} = \frac{106.401C_r}{(1 + 106.401C_r)^{1.548} \frac{1}{1.548} (1 - C_r)^{0.278}}$
15	$\frac{q}{q_m} = \frac{134.461C_r}{(1 + 134.461C_r)^{1.426} \frac{1}{1.426} (1 - C_r)^{0.336}}$
20	$\frac{q}{q_m} = \frac{160.005C_r}{(1 + 160.005C_r)^{1.335} \frac{1}{1.335} (1 - C_r)^{0.388}}$
25	$\frac{q}{q_m} = \frac{183.827C_r}{(1 + 183.827C_r)^{1.262} \frac{1}{1.262} (1 - C_r)^{0.437}}$
30	$\frac{q}{q_m} = \frac{206.362C_r}{(1 + 206.362C_r)^{1.021} \frac{1}{1.021} (1 - C_r)^{0.483}}$
35	$\frac{q}{q_m} = \frac{227.878C_r}{(1 + 227.878C_r)^{1.149} \frac{1}{1.149} (1 - C_r)^{0.528}}$
40	$\frac{q}{q_m} = \frac{248.561C_r}{(1 + 248.561C_r)^{1.102} \frac{1}{1.102} (1 - C_r)^{0.572}}$

Table 4.27 The predicted adsorption isotherms for alumina at various degrees of deactivation

Alumina	
% Deactivation	Equations
5	$q = 1.057C^{0.830}$
10	$q = 0.9261C^{0.836}$
15	$q = 0.806C^{0.848}$
20	$q = 0.695C^{0.868}$
25	$q = 0.595C^{0.896}$
30	$q = 0.504C^{0.936}$
35	$q = 0.424C^{0.986}$
40	$q = 0.353C^{1.049}$

4.7 Breakthrough Curves

The proper time to operate the adsorption steps that made the product meet with acceptable specification was revealed by concentration of water at the outlet. The plot between the concentration of water at the outlet as a function of time of operation can be called as breakthrough time, which can be obtained from both the experiments and theorem. In this work, both of them are shown and compared.

4.7.1 Experimental Breakthrough Curves

From the experiments designed by Chaikasetpaiboon, (2002), using the same conditions as in Khaikham's work, the natural gas was fed to the system with the flow rate of 457.8ml/min and mixed with the water until the 30% relative humidity was reached before being fed into the adsorber packed with the three types of adsorbents. The content water at the outlet changing with the time of operation is shown in Figure 4.30, indicating that the breakthrough time is about 30.3 hours. Moreover, the breakthrough time for deactivated adsorbents was investigated by using the same condition as applied to fresh adsorbents, but the adsorber in this case was packed with 88.3% deactivated alumina, 73.75% deactivated 1/8" molecular

sieve, and 82.95% deactivated 1/16" molecular sieve. Figure 4.31 shows that the breakthrough time is about 1.75 hours.

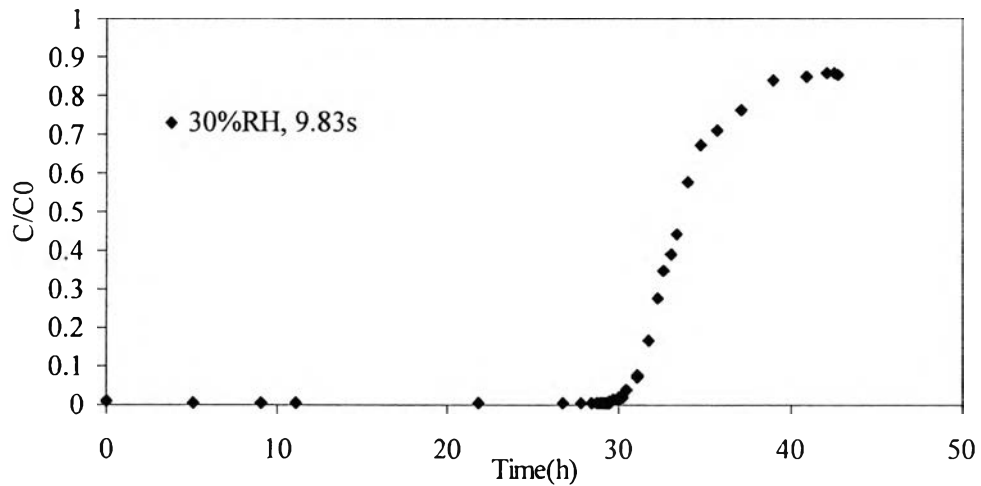


Figure 4.30 Experimental breakthrough curve for the fresh adsorbents packed in the adsorber.

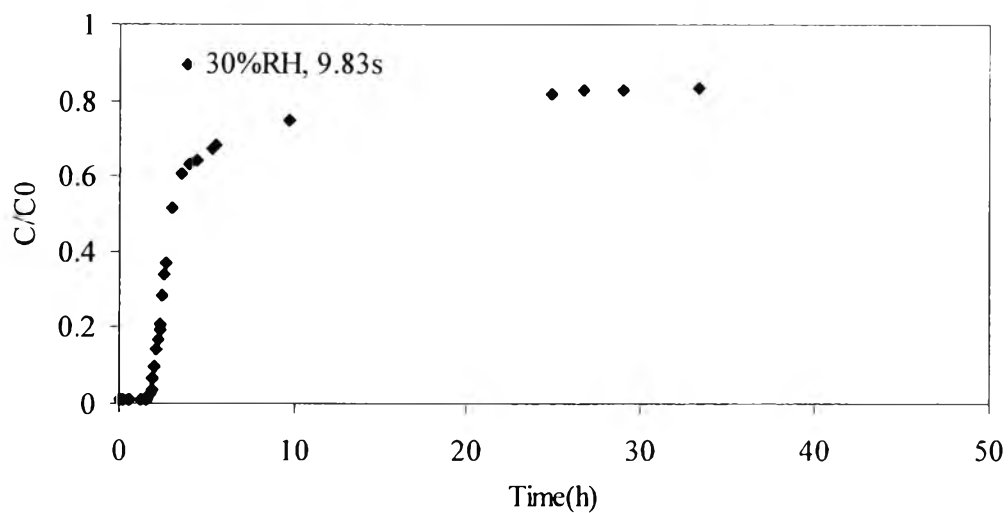


Figure 4.31 Experimental breakthrough curve for the adsorber packed with 88.3% deactivated alumina, 73.75% deactivated 1/8" molecular sieve, and 82.95% deactivated 1/16" molecular sieve.

4.7.2 Theoretical Breakthrough Curves

In this part, the mathematical model for prediction the breakthrough time was developed from the Uttamaroop (2003)'s work by including the effect of the pressure drop that had been neglected in his work. Moreover, the mass transfer coefficient previously kept constant for all degrees of deactivation was instead varied with the degree of deactivation for each adsorbent.

4.7.2.1 *Comparison of Experimental and Theoretical Breakthrough Curves of Adsorber Packed with All Fresh Adsorbents*

Figure 4.32 below shows the comparison of breakthrough curve between the experiment and theorem. The mass transfer coefficient for each type of adsorbent is $k_1 = 6.23 \times 10^{-5} \text{ s}^{-1}$, $k_2 = 4.48 \times 10^{-5} \text{ s}^{-1}$, and $k_3 = 1.58 \times 10^{-5} \text{ s}^{-1}$, for alumina, 1/8" Molecular sieve, and 1/16" Molecular sieve, respectively.

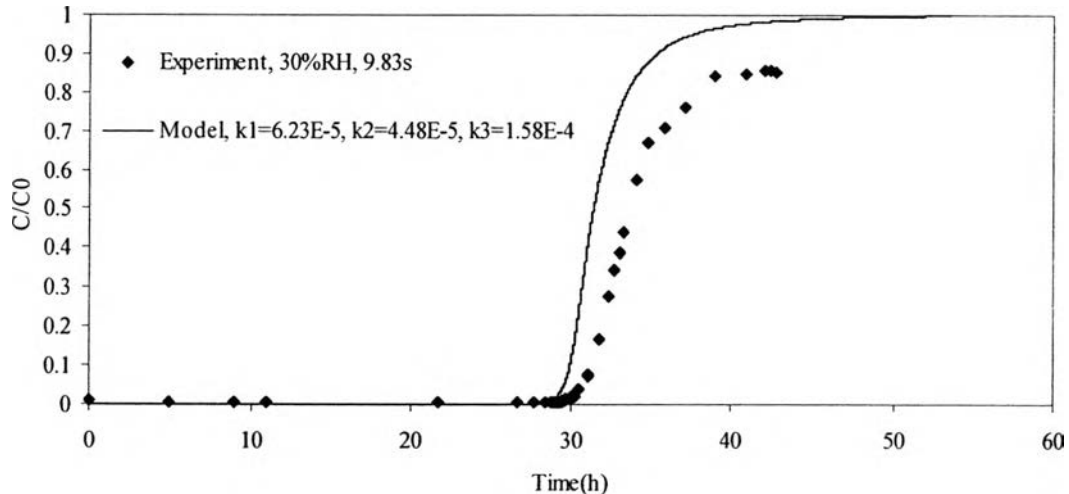


Figure 4.32 Comparison between the experimental and theoretical breakthrough curves of the adsorber packed with all fresh adsorbents.

Figure 4.32 shows that the breakthrough time from the theorem is about 29.1 hours, which is shorter than that from the experiment about 1.2 hours.

4.7.2.2 Comparison of Experimental and Theoretical Breakthrough Curves of Adsorber Packed with a Set of Deactivated Adsorbents

The adsorption isotherm and the parameters varied with deactivation such as void fraction, ϵ , mass transfer coefficient, k , were applied in the governing equation. Moreover, the increase of pressure drop affecting to the interstitial velocity profile along the adsorber was applied to the model in order to predict the theoretical breakthrough time also. The comparison of the experimental and theoretical breakthrough time is shown in Figure 4.33.

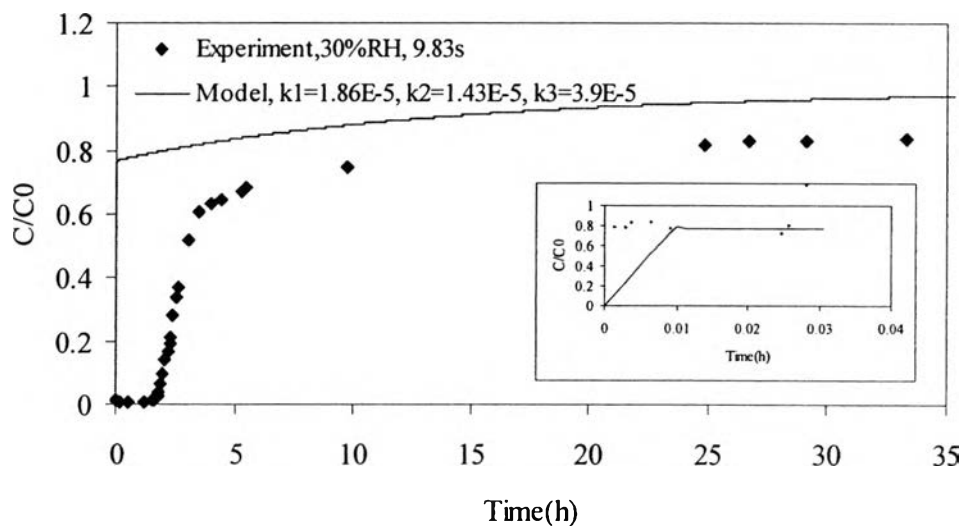


Figure 4.33 Comparison between the experimental and theoretical breakthrough curves for the case of deactivated adsorbents (88.3% deactivated alumina, 73.75% deactivated 1/8" molecular sieve, and 82.95% deactivated 1/16" molecular sieve).

From the Figure 4.33, the breakthrough time from the theorem fast occurs at the time of operation or approximate 0 hour shorter than the experiment about 1.75 hours and the trend of curve is still in accordance with the experiment as in the case of fresh adsorbent.

4.8 Sensitivity of Each Deactivated Adsorbent on the Breakthrough Time

The sensitivity of deactivated adsorbents on the breakthrough time was studied by the previous work, but it was limited to the low degrees of deactivation, so the change of breakthrough time at all degrees of deactivation was completed in this work. Figure 4.34 shows the relationship between the breakthrough time ratio (the breakthrough time of a deactivated bed divided by the breakthrough time of fresh bed) and the deactivation ratio (the adsorption capacity of deactivated adsorbents subtracted by the adsorption capacity of fresh adsorbents and then divided by the adsorption capacity of fresh adsorbents), which each line represents the deactivation ratio at various degrees of deactivation when an adsorbent was deactivated whereas the rest was kept fresh.

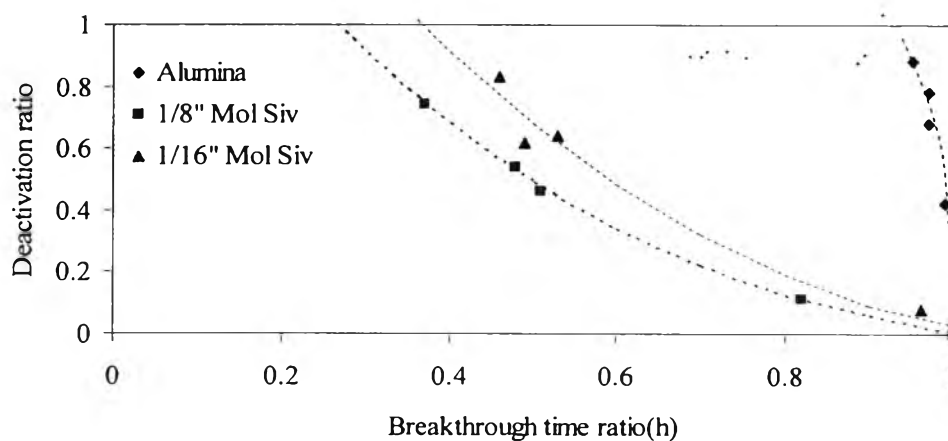


Figure 4.34 Relationship of deactivation ratio and theoretical breakthrough time ratio for each adsorbent when it was deactivated whereas the rest was kept fresh.

The curves show that the deactivation of 1/8" molecular sieve affects on the breakthrough time the most, which is opposite to alumina whose deactivation has little effect to the breakthrough time. Even through, alumina is deactivated to about 80%, the breakthrough time is not significantly changed. However, from the curve, it shows that at 100% deactivation (deactivation ratio equals to 1) for each adsorbent the breakthrough time ratio does not decrease to zero because another two layers are still fresh, so the adsorption still occurs.

4.9 Predicted Breakthrough Time for any Composition

As explained in Khaikham's work, the alumina have trend to easily be deactivated more than the molecular sieve, And from the experiments, the adsorbent was prepared to the various degrees of deactivation represented by notations as shown in Table 4.28. So, the possible combinations of packed beds in the adsorber are shown in Table 4.29.

Table 4.28 Notation representing the various degrees of deactivation for each adsorbent.

Adsorbent	%Deactivation	Notation
Alumina	0	F _A
	42.46	D _{1A}
	67.92	D _{2A}
	77.97	D _{3A}
	88.3	D _{4A}
Molsiv (1/8")	0	F _{UIB}
	11.36	D _{1UIB}
	46.24	D _{2UIB}
	53.98	D _{3UIB}
	73.75	D _{4UIB}
Molsiv (1/16")	0	F _{UIS}
	7.96	D _{1UIS}
	62.39	D _{2UIS}
	63.96	D _{3UIS}
	82.95	D _{4UIS}

Table 4.29 Predicted breakthrough time of the possible combinations of packed beds in the adsorber

Alumina	Molsiv (1/8")	Molsiv (1/16")	Breakthrough time(h)
F _A	F _{UIB}	F _{UIS}	29.1
D _{1A}	D _{1UIB}	D _{1UIS}	21.3
D _{2A}	D _{1UIB}	D _{1UIS}	20.9
D _{2A}	D _{2UIB}	D _{2UIS}	0.83
D _{2A}	D _{3UIB}	D _{3UIS}	0
D _{3A}	D _{1UIB}	D _{1UIS}	20.7
D _{3A}	D _{2UIB}	D _{2UIS}	0.79
D _{3A}	D _{3UIB}	D _{3UIB}	0
D _{4A}	D _{1UIB}	D _{1UIB}	20.7
D _{4A}	D _{2UIB}	D _{2UIS}	0
D _{4A}	D _{3UIB}	D _{3UIB}	0
D _{4A}	D _{4UIB}	D _{4UIB}	0

From above table, it shows that the breakthrough time decreases almost at the beginning of operation time when the 4A molecular sieves deactivate to about 54%. And at the same degrees of deactivation of the 4A molecular sieves, the breakthrough time does not change much as the deactivation of alumina increases as mentioned before.

4.10 Predicted Breakthrough Time from Predicted Adsorption Isotherms

Using the predicted adsorption isotherms, the theoretical breakthrough time for various beds composed of deactivated adsorbents in combinations can be predicted. For ease, every adsorbents was assumed to be at the same degree of deactivation as shown in Table 4.30 below. However, the program can give results for all combinations.

Table 4.30 Notation of any combination of adsorbents in the adsorber

Material	Alumina	Molsiv (1/8")	Molsiv (1/16")	Notation
%Deactivation	5	5	5	D5
	10	10	10	D10
	15	15	15	D15
	20	20	20	D20
	25	25	25	D25
	30	30	30	D30
	35	35	35	D35
	40	40	40	D40

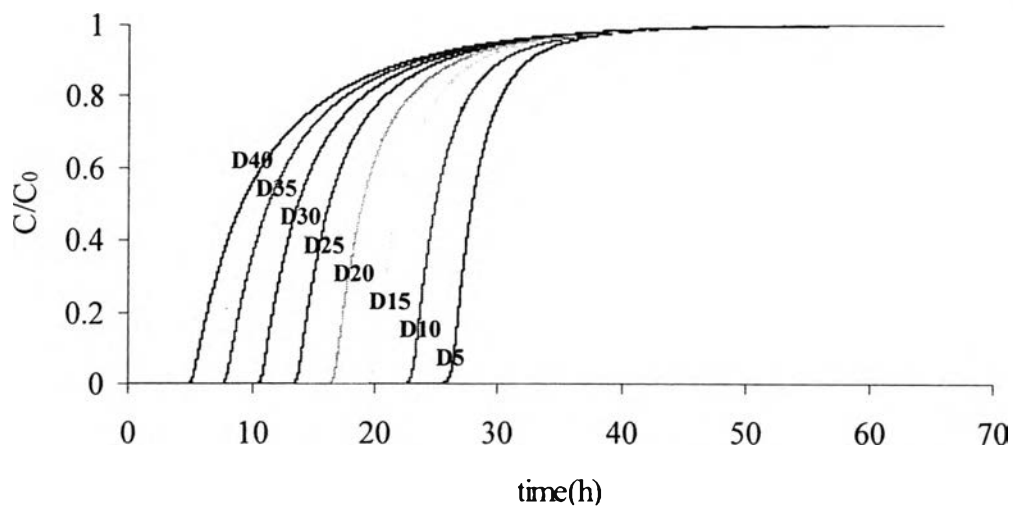
**Figure 4.35** Change of breakthrough curve using predicted adsorption isotherms at various degrees of deactivation.

Figure 4.35 shows the change of the theoretical breakthrough time, indicating that it decreases when the degree of deactivation increases. Moreover the curve shows that the slope of water content at the outlet at the lower degrees of deactivation is steeper than at the higher degree of deactivation since the adsorbents at lower degrees of deactivation have higher mass transfer coefficient than the higher degrees. For the lower slope of curve (lower mass transfer coefficient), it means that

the mass transfer zone is long. So, when the front of mass transfer zone reaches to the outlet or at breakthrough time, the adsorbents are not saturated yet. Conversely, for the higher slope (higher mass transfer coefficient), it means that the mass transfer zone is short. So, when the front of mass transfer zone reaches to the outlet or at breakthrough time, the almost of adsorbents is saturated with water.